Green Chemical Technology

SCIEPublish

Review

Immobilization Strategies of Cyclodextrins on Ferrimagnetic Nanoparticles for Dye Water Remediation: A Review

Géraldine Gouhier [1,*], Cécile Barbot [1] and Brian D. Wagner [2]

[1] Institut CARMeN UMR 6064, University Rouen Normandie, INSA Rouen Normandie, University Caen Normandie, ENSICAEN, CNRS, IRCOF, 1 Rue Tesnière, 76821 Rouen, France; cecile.barbot@univ-rouen.fr (C.B.)

[2] Department of Chemistry, University of Prince Edward Island, Charlottetown, PE C1A 4P3, Canada; bwagner@upei.ca (B.D.W.)

* Corresponding author. E-mail: geraldine.gouhier@univ-rouen.fr (G.G.)

Received: 5 March 2026; Revised: 28 April 2026; Accepted: 18 May 2026; Available online: 29 May 2026

ABSTRACT: This paper provides a comprehensive review of the synthesis, use, and advantages of cyclodextrin-derivatized ferrimagnetic nanoparticles for the removal of textile dyes from natural waters. Dyes make their way into natural water systems and affect ecosystems and human health. Water soluble natural cyclodextrins (CD) are able to include dyes into their hydrophobic cavities. To extract the pollutant from water, the host molecules need to be tethered to insoluble supports, such as magnetic nanoparticles, making possible the extraction of the pollutant from the water using a simple magnet. Thus, after washing treatment, the pollutant is extracted, and the support is regenerated for a new remediation cycle. We report herein the synthetic strategies to immobilize β-cyclodextrin onto magnetic nanoparticles MNP@CD using weak to strong bindings, and the analytical methods used to characterize and monitor their effectiveness. Hydroxyl groups present on the CD scaffold can chelate iron cores by coprecipitation, solvothermal reaction, polymerization, carboxylic acid coordination, and silica bonding. An assessment of various dye adsorption capacities of MNP@CD is reported, spanning a range of 3 orders of magnitude, from 2.38 to 2780 mg of dye/g. The recyclability of the magnetic nanoparticles, with excellent removal rates of 90% after a few cycles, is also discussed.

Keywords: Magnetic nanoparticle; Cyclodextrin; Industrial dyes; Wastewater remediation; Ferrimagnetic; Host-guest inclusion; Silica coating; Co-precipitation

1. Introduction

Textile manufacturing and clothing production are large and important industries in many countries around the world. However, along with their enormous positive economic activities comes a large negative impact on the environment. These industries use a wide range of dyes to achieve the desired palette of colors, including dyes arising from natural sources and, more recently, synthetic dyes. These dyes enter natural water systems, where they can adversely affect ecosystems and human health in various ways, as discussed below.

Many of these dyes, contained in industrial effluents and household washings, have dramatic detrimental effects on the environment, not only on the health of aquatic species, but also on drinking water quality and safety. Islam et al. recently published a comprehensive review on the impact of textile dyes on human health and the ecosystem [1]. They point out that the textile industry is a major contributor to water pollution, due to its large consumption of water in its industrial processes and the discharge of coloring agents into natural water systems. The release of effluents from the textile industry has major impacts affecting many aspects of aquatic health, including biological oxygen demand (BOD), total dissolved solids, toxic compounds, and pH [1]. These factors can significantly negatively affect both aquatic species populations and human health. Azo dyes, for example, which represent an important category of dyes used in the textile industry, are known to be human carcinogens [2].

There have been numerous approaches to the remediation of industrially polluted natural waters, including specifically the removal of dyes from wastewater [3,4]. Various materials that adsorb pollutants have been applied, including graphene-based catalysts [5], but the most widely utilized materials for pollutant removal are those involving cyclodextrins [6–10]. Cyclodextrin-based materials have been applied to the removal of a wide range of water pollutants, including pesticides and heavy metals [11], perfluoroalkyl compounds [12], and textile dyes [7,10,13–15]. In such applications, the cyclodextrin host molecules need to be tethered to some sort of material support, such as polymers [6,7,13] or magnetic nanoparticles [16], to allow for removal of the dye molecules and recovery of the adsorbent material. Magnetic nanoparticles have also been applied to other areas, including biomedical frontiers [17], protein immobilization [18], and MRI [19]. This paper provides a comprehensive review of the synthesis, the use, and the advantages of cyclodextrin-derivatized ferrimagnetic nanoparticles for the removal of textile dyes from natural waters.

1.1. Textile Dyes: Their Use and Contamination of Natural Waters

Dyes have been used to color clothing since ancient times [20]. One of the earliest dyes used is indigo, whose structure is shown in Figure 1a. Indigo, which in fact is the origin of the name of this vibrant color, is a natural dye that has been produced by various cultures around the world. It is a strong, deep blue dye with a multitude of uses. Methylene blue is an example of a highly used synthetic dye; its structure is shown in Figure 1b. Benkhaya et al. have provided a useful review on the classification, synthesis, and uses of textile dyes [21]. The wide range of natural and synthetic dyes can be categorized in different ways, such as based on functional groups or based on the method of application [21].

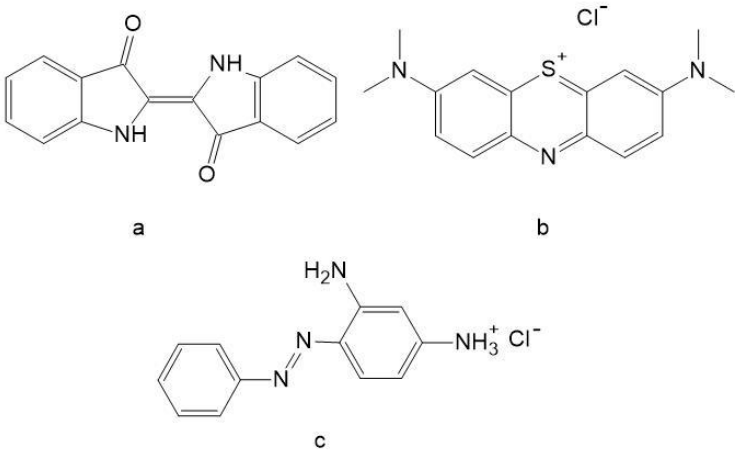

Figure 1. The chemical structure of three representative textile dyes: (**a**) indigo; (**b**) methylene blue; (**c**) basic orange 2.

All molecules that are useful as dyes have certain properties in common, including strong absorption in the visible region, resulting in bright colors from the transmitted light, chemical and photochemical stability, and the ability to bind onto materials. Alegbe et al. provide a practical definition of dyes, which is useful for the purposes of this review: "dyes can be defined as chromophoric substances with a capacity to interact chemically or physically with substrates, leading to selective absorption of specific wavelengths of light and resulting in a display of color" [20]. Since dyes work through light absorption, it is important to note that the color of the dye is a result of the part(s) of the visible spectrum which are not absorbed; a color wheel is useful for relating the absorption spectrum of dyes to their observed color. Textile dyes enter the environment in several ways, most predominantly through industrial effluents from factories producing the dyes as well as the dyed clothing. However, household washing of dyed clothes is also a significant source, as is the disposal of used clothing in landfills and other waste destinations. The latter source is exacerbated by the recent rise of "fast fashion", the large-scale production of relatively cheap clothing which is poorly made and destined for rapid disintegration and disposal [22,23], significantly contributing to the sources of dyes into the environment Azo dyes, a common category of synthetic dyes, are known human carcinogens [2]. An example of a highly used azo dye that makes its way into natural water systems is basic orange 2, the chemical structure of which is shown in Figure 1c; the azo group (-N=N-) is readily apparent in the center of the molecule. Bazin et al. studied the estrogenic and anti-estrogenic activity of 23 commercial textile dyes and found that around half of the azo dyes showed strong anti-estrogenic activity, and hence are potential endocrine-disrupting agents, which will negatively impact aquatic species such as fish [24]. In their 2023 review of the impact of textile dyes on human and ecosystem health, Islam et al. provide extensive tables of specific textile dyes and their specific human and aquatic species health impacts [1]. It is clear that textile dye pollution represents a massive and consequential threat to the environment.

Dye-contaminated natural waters are challenging to remediate for a variety of reasons. Many dyes, particularly cationic ones such as methylene blue and basic orange 2 (see Figure 1), are highly water soluble. Dye-containing effluents are often a complex mixture of various dyes and other organic pollutants. Also, such effluents are often also contaminated with heavy metals [1]. The removal of such dyes requires an adsorbent material that can trap the dye molecules, then release them for capture. The adsorbent material needs to be able to be cycled many times, with minimal degradation, and recoverable from the water. Solid matrices such as polymeric materials are one solution. A more interesting group of materials is magnetic nanoparticles; once the dye molecules are trapped on the nanoparticles, they can be removed, recovered, and washed using a simple magnet. This approach consists of grafting cyclodextrin host molecules to the nanoparticle surface. The role of cyclodextrins as molecular hosts to trap dyes and the preparation of cyclodextrin-decorated magnetic nanoparticles will be introduced in the next two sections.

1.2. Cyclodextrins as Hosts for Dye Inclusion

Cyclodextrins (CDs), cyclic oligomers of glucopyranose, are by far the most utilized macrocyclic molecular hosts [25]. They are able to form supramolecular host-guest inclusion complexes with a wide range of neutral and ionic guest molecules, making them versatile and highly applicable hosts [26]. There is a long history of cyclodextrin use as host molecules, beginning with their first discovery in the 1890s [27]. They have found significant applications in a wide range of fields, including health, food, agriculture, and industry [28]. They have been applied in the development of magnetic solid phase extraction methods [29]. They have also played an important role in the textile industry itself, for example, as auxiliary agents in the dyeing process [30]. There are three commonly available native cyclodextrins, α-, β-, and γ-cyclodextrin, containing 6, 7, or 8 glucopyranose monomers, respectively. However, the presence of hydroxyl groups (3 per glucopyranose unit) allows relatively easy derivatization of these native hosts, yielding a wide array of modified cyclodextrins available for use. Figure 2 shows the chemical structure of

modified β-cyclodextrin, where R is often an alkyl group such as methyl, and for native (unsubstituted) β-cyclodextrin, R = H.

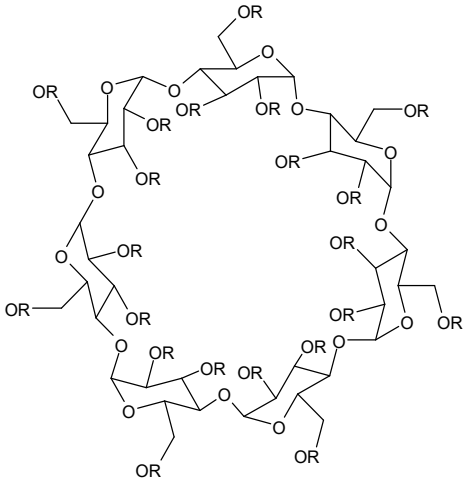

Figure 2. The chemical structure of modified β-cyclodextrin.

Host-guest inclusion complexes occur in solution when a dissolved guest molecule becomes encapsulated within the internal cavity of a larger host molecule,, such as a cyclodextrin [31]. This inclusion within the host cavity results in significant changes to the guest properties, including solubility, stability, reactivity, and spectroscopic properties such as fluorescence intensity [31]. If the hosts are attached to a matrix, such as a polymer, is it possible to trap these guest molecules and thus remove them from a solution, such as polluted water? Alternatively, if the cyclodextrins are attached to magnetic nanoparticles, then once the guests are bound to the cyclodextrins, the loaded particles can be removed from the solutions using a magnet. This is the idea behind using cyclodextrin-derivatized ferrimagnetic nanoparticles to remove dye pollutants from textile-industry contaminated natural waters, which will be explored in Section 1.3. Before examining this approach in detail, it is first important to discuss the binding of dye molecules by free cyclodextrins in aqueous solution. The most important property describing the binding of a guest in a molecular host is the binding constant, sometimes referred to as the association constant, K. Assuming a 1:1 host-guest binding complex, in which a single guest (G) becomes encapsulated within a single host (H), the binding process can be simply written as the following equilibrium:

$$H + G \rightleftharpoons \{H:G\} \quad (1)$$

where {H:G} represents the host: guest complex. For such a simple 1:1 binding, K is given by the equation:

$$K = [\{H:G\}]/[H][G] \quad (2)$$

K has a unit of M^{-1}, and the stronger the binding, the higher the value of K. The magnitude of K is indicative of the Gibbs Energy change for the inclusion process, which has both enthalpic and entropic contributions [31]. This is often discussed in terms of the driving forces for inclusion. Such driving forces in aqueous solution include van der Waals interactions, hydrogen bonding, and the hydrophobic effect, and depend on the specific guest and host, their size and shape match, and electronic properties [31].

Various experimental techniques can be used to obtain the binding constant, with spectroscopic techniques being the most common. The extraction of the value of the binding constant K involves various data analysis techniques and has been discussed in detail in reference [31]. There have been a number of experimental studies on the binding of relevant dye molecules by cyclodextrins in aqueous solution, with a range of K values reported for different dye molecules. These studies will be reviewed in Section 3.

1.3. Magnetite Structure and Its Magnetic Properties

Magnetite, Fe_3O_4, is the magnetic support used to immobilize cyclodextrins in the dyes remediation strategy. We will describe herein the physical origin of its magnetism property. This iron particle crystallizes in an inverse spinel structure (AB_2O_4), in the cubic Fd-3m space group, with A and B representing, respectively, tetrahedral and octahedral sites. The unit-cell (Figure 3) is formed of eight cubic units with a lattice parameter of 8.39 Å [32]. There are, in the unit cell, 64 tetrahedral sites (sites A) and 32 octahedral sites (site B) with iron surrounded in each of them by oxygen atoms. Two cation sites are observed in the structure: Fe(III) occupies tetrahedral sites (8 per unit cell, which represents 1/8 of the tetrahedral sites), and Fe(III) and Fe(II), in equal amounts, occupy octahedral sites (16 per unit cell, which represents 1/4 of the octahedral sites for each of them). Magnetite's unit cell can also be represented with the formula $(Fe(III))_8$ $[Fe(II, III)]_{16}$ O_{32} where the parentheses stand for tetrahedral sites and the brackets for octahedral sites. The high electrical conductivity observed in magnetite, in comparison to other ferrimagnetic oxides, can be explained by the rapid hopping of electrons between Fe(II) and Fe(III) ions in site B, through a direct double exchange interaction [33,34] (Figure 4a). The spin down electron can only hop from $Fe(II)_{Oh}$ to $Fe(III)_{Oh}$ if the majority spins are the same. Hence, they are coupled and aligned in parallel. The magnetic properties arise from the arrangement of the spins of Fe(III) in tetrahedral sites (sites A), which are antiparallel coupled with Fe(II) and Fe(III) from octahedral sites (sites B), the latter being much more numerous. This antiferromagnetically coupling generates, through a super-exchange effect (Figure 4b) via O(-II) anions (so not directed between two iron atoms), a ferrimagnetic material (Figure 5) with high saturation magnetization (M_s) and low coercivity (H_c). In this process, the spin-up 5d electrons in the $Fe(III)_{Oh}$ couple with the overlapping 2p orbitals in the O(-II), making them spin-down. The other 2p electron is thus spin-up, which makes the $Fe(III)_{Td}$ 5d electrons spin-down. Thus, $Fe(III)_{Oh}$ and $Fe(III)_{Td}$ are antiparallel and cancel out their unpaired spin magnetic moments. Therefore, all the Fe(II) cations contribute to the magnetic moment, while all the Fe(III) cancel each other. Additionally, magnetic particles with sizes less than 30 nm, with zero coercivity (the field required to bring the magnetism to zero) and zero remanence (residual magnetization) exhibit superparamagnetism. In other words, by applying an external magnetic field, they become magnetized up to their saturation magnetization, and after removal of this applied magnetic field, they do not retain any magnetism. Different from large magnets, these nanoparticles do not exhibit multiple magnetic domains, but rather, a single magnetic domain that acts as a "single super spin" that exhibits high magnetic susceptibility. These nanoparticles provide a stronger and more rapid magnetic response in comparison to that of bulk magnets, after application of a magnetic field. Thus, these properties facilitate the separation of the dyes immobilized on magnetite nanoparticles from liquid solutions using a magnet.

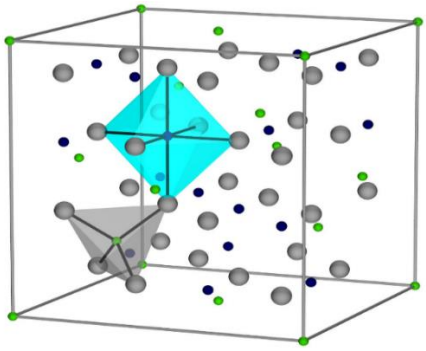

Figure 3. Crystal structure of Fe_3O_4 Magnetite, with oxygen atoms in gray, Fe^{3+} ions in green (occupying the tetrahedral and octahedral sites) and Fe^{2+} ions in blue (occupying the octahedral sites).

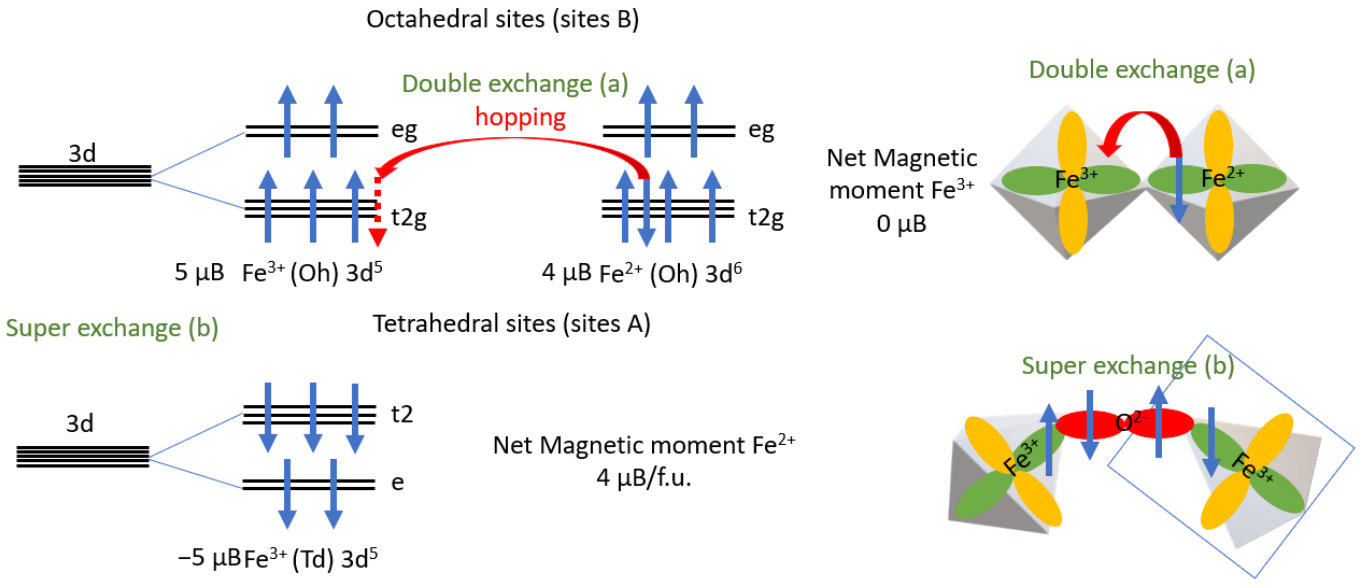

Figure 4. The possible configuration of the Fe(II) and Fe(III) cations in the Oh and Td coordination in Fe_3O_4 in high spin. (**a**) Double exchange: hopping between the d-orbitals from Fe(II) and Fe(III) cations on the Oh sites ; spins are coupled and aligned in parallel. (**b**) Super exchange between Fe(III) Oh and Fe(III) Td cations. Fe(III) Oh and Fe(III) Td are antiparallel and cancel out their unpaired spin magnetic moments. Therefore, all the Fe(II) cations contribute to the magnetic moment, while all the Fe(III) cancel each other. Net magnetic moment expressed in Bohr magneton/f.u. (formula unit).

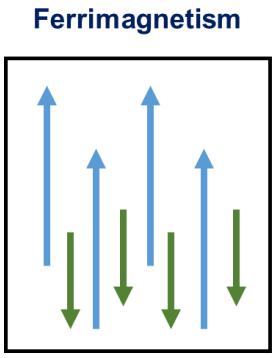

Figure 5. Illustration of ferrimagnetic properties induced by the magnetic moments of an inorganic structure. Ferrimagnetic materials hold a spontaneous magnetization below the Curie temperature with spins which are aligned antiparallel but do not cancel.

1.4. Ferrimagnetic Nanoparticles in Water Remediation

Natural water remediation by magnetism involves adding a magnetic sorbent to a contaminated solution. After an appropriate mixing time, the pollutant is adsorbed by chemo- and/or physisorption onto the insoluble nanoparticles. The liquid/solid separation is possible by simple magnetization using an external magnet. The depolluted water is extracted, and the magnetic nanoparticle (MNP) is desorbed by a chemical treatment to release the pollutant in its concentrated form. Thus, the MNP is regenerated for a new remediation cycle. Compared to active charcoal or resin/membrane supports, such an easy and convenient extraction process avoids clogging of the pumps and the need for high pressure. Moreover, the low cost of magnetite materials and the recyclability of the support are two other advantages compared to the expensive synthesis of functionalized polymers or the high energy consuming synthesis of activated carbon. Lastly, the recyclability of the MNP limits the highly energetic incineration needed for the other two supports when they are saturated at the end of life. Consequently, the use of magnetic sorbents is time-saving, cost-effective, and environmentally friendly.

Magnetite is well described as a good nano-adsorbent. This insoluble iron nanoparticle, Fe_3O_4, results from the combination of ferrous ions Fe^{2+} (1/3) and ferric ions Fe^{3+} (2/3), giving the formula $Fe(II)Fe(III)_2O_4$. The crystal stacking of these nanoparticles generates ferrimagnetic properties. Two approaches are possible to obtain magnetic nanoparticles (MNP) [35,36]. The first one is based on a physical process using raw materials (metals, oxides, ores), which are reduced to powder by grinding or laser ablation, and high polydispersity is observed. The second one is a chemical method starting from atoms, such as the most popular co-precipitation and the hydrothermal reactions. Co-precipitation involves simultaneously precipitating ferrous ions and ferric ions in the presence of an alkaline solution, according to the reaction.

$$FeCl_2 \cdot 4H_2O + 2FeCl_3 \cdot 6H_2O + 8NH_4OH \rightarrow Fe_3O_4 + 8NH_4Cl + 20H_2O \quad (3)$$

This method is widely used, and good high purity yields with accurate stoichiometric phases are obtained. The simplicity of implementation makes large-scale transfer possible. If the average size of nanoparticles between 1 and 100 nm can be controlled, the size distribution remains high. Moreover, the use of aqueous ammonia increases the risks for humans in case of industrial accidents. The use of weaker bases remains possible, but at the expense of the precipitation kinetics. The hydrothermal pathway is the oldest method of manufacturing magnetite. It requires the presence of iron salts in an aqueous medium; the solution is brought to high temperature (200–250 °C) in an autoclave maintained under high pressure (0.1 MPa or atmospheric pressure at 14 MPa) for 24 to 72 h. When the supercritical conditions of water are reached, ferrous ions form intermediate hydroxides that can be transformed into iron oxide by dehydration. This way of synthesis requires expensive equipment, and the results are often not reproducible.

Pure magnetite nanoparticles have some limitations for use because they tend to oxidize to maghemite (γ-Fe_2O_3) or even hematite (α-Fe_2O_3) in air and to agglomerate, leading to a decrease or complete loss of magnetic properties. This is the reason why it is often necessary to cover the magnetic core with a protective layer, called a coating, to ensure its stability over time. The main coatings described are based on organic or inorganic polymers, surfactants, or bio-based molecules such as silica [37,38], polydopamine [39], ionic liquids [40], and cyclodextrins. Depending on the required function of the strategy, the stability and the thickness of the coating can vary and reduce the magnetization properties of the nanoparticles [41]. As this review is focused on MNP functionalized by cyclodextrin (CD) scaffold, additionally, this synthesis step can be a way to introduce other chemical functions onto the Fe_3O_4 nucleus to improve the capture capacity of pollutants such as polymers [42], polysaccharides [43], ionic liquids [44], nanotubes [45], graphene oxide [46], and nanosponges [47]. Thus, decorated MNP@CDs have been used as adsorbents for heavy metals [48], radionuclides, pathogens, and organic pollutants such as polycyclic aromatic hydrocarbons (PAHs), aromatic amines, chlorophenols, bisphenol A, phenol and hydroquinone, phthalate esters, pesticides, *etc*. [9,11]. For instance, the capture of dye molecules has been reported using ligands that bind contaminants via coordination, acid-base reactions, or dipole-dipole interactions. This review aims to highlight the synergic effect of the use of magnetic nanoparticles functionalized with β-cyclodextrins to extract and concentrate dyes present in waste waters by simple magnetic filtration using additional host-guest supramolecular interactions. A few other reviews have been published in recent years that involve related topics, but are distinct in focus and content from this current review. Mishra et al. in 2021 reported water dye adsorption using nanomaterials and magnetic nanoparticles, and detailed isotherm modeling and kinetic studies, considering various factors such as pH, dye concentration, adsorbent amount, and temperature. Removal efficiency increases with adsorbent concentration but declines sharply with increasing pH [49]. Nojavan et al. reported the immobilization of CD onto different supports, such as graphene oxide, POSS, and MNP to produce nanosponges and hybrid substances for magnetic solid phase extraction (MSPE) of organic compounds and heavy metal ions from biological, environmental, and food samples [29]. Li et al. in 2024 published a review dedicated to the removal of contaminants such as dyes and metals by CD

adsorbents such as cross-linked polymers, nanosponges, fibres, membranes, graphene oxide, and TiO_2 [9]. They used a statistical analysis by scrutinizing 2038 articles from 1993 to 2022 and did not focus the study on MNP@CD support. In contrast, this review will be focused on the published references on cyclodextrins and polymers of cyclodextrins with iron magnetic nanoparticles by detailing the possible chemical immobilization strategies and the capture capacities by families of dyes. It will be emphasized that these materials can be reused for another remediation cycle, leading to an economical circular process.

2. Results: Immobilization of Cyclodextrins on Magnetic Nanoparticles

We report herein five strategies to immobilize β-cyclodextrin macrocycles onto magnetic nanoparticles MNP@CD using weak to strong bindings. Hydroxyl groups present on the CD scaffold can chelate the iron core by coprecipitation, solvothermal reactions, polymerization, carboxylic acid coordination, and silica bonding. The adsorption/desorption mechanisms involved between charged organic dyes molecules and MNP@CD are multiple and include electrostatic interaction, hydrogen bonding, host-guest inclusion complexation, and ion exchange, leading to the enhancement of the adsorption capacity. Consequently, for accuracy, the term adsorption will refer to the process of immobilizing a dye onto a support material. It includes one or several mechanisms described previously, including physical adsorption. The MNP@CD are characterized by many complementary analysis such as Fourier transform infrared (FTIR) to validate the presence of chemical functionalization, zeta potential to determine the surface charge, X-ray diffraction (XRD) to evaluate the crystallinity, and dynamic light scattering (DLS) to measure the particle diameter. Electron microscopies are used to image the shape, size, and calculate the elemental composition; these include scanning electron microscopy (SEM), atomic force microscopy (AFM), and transmission electron microscopy (TEM). The magnetic properties of the synthesized MNP@CD are measured through a vibrating-sample magnetometer (VSM), and the performance of magnetic materials can be assessed by hysteresis loop determinations at ambient temperature. The hydrodynamic diameter was determined using dynamic light scattering experiments. For instance, by XPS the characteristic diffraction peaks of bare Fe_3O_4 at $2\theta \approx 32°$, 37°, 43°, 53°, 57° and 63° correspond to a cubic spinel structure with (220), (311), (400), (422), (511) and (440) planes, respectively, and did not change with immobilization of CD onto the magnetic support. FTIR provides useful characterization information on MNPs at the various stages of synthesis. Characteristic IR bands from the literature are listed in Table 1 for MNP, coated MNPs, and MNP@CD. By FTIR, the absorption band related to the Fe–O–Fe vibrations is variable from 537 to 656 cm^{-1}. The presence of cyclodextrin on the iron nanoparticle can be observed with peaks at around 1025 and 1161 cm^{-1} attributed to C–C/C–O conjugated stretching and the C–O–C antisymmetric glycosidic vibrations, respectively. The O–H stretching and C–H asymmetric vibrations appear as broad bands at 3500–3300 and 2925 cm^{-1}, respectively. There is a correlation between the ratio between iron and organic coating and the magnetic properties, with the presence of organic matter causing a decrease in saturation magnetization. However, even low magnetization values can produce efficient magnetic adsorbents to easily separate the nanoparticles from aqueous media. The use of an external magnet generates a fast aggregation and a rapid redispersion after shaking once the magnetic field is removed. TGA experiments on the adsorbents provide an estimate of the amount of β-CD coating on the iron NPs by monitoring the weight loss of the material. Total weight loss of bare Fe_3O_4 is about 2.4% due to the dehydration of the surface and loss of the absorbed water molecules at below 130 °C. Then, oxidation of Fe_3O_4 to Fe_2O_3 occurs at 130 °C and 215 °C. In the presence of MNP@CD, two weight loss steps appear of about a few % below 200 °C due to adsorbed water evaporation or hydrogen-bonded water molecules. Then, a percentage of weight loss can be observed in the temperature range from 200 to 450 °C, attributed to the thermal decomposition of the β-CD layer and corresponding to the quantity of CD coating on the iron particles. Zeta potential measurements as a function of pH determine the charge on the magnetic nanoparticle surface and predict possible interactions with anionic or cationic dyes. The isoelectric point (IEP) or point of zero

charge pH_{zpc} corresponds to the pH at which the net surface charge of a solid is equal to zero. This value is pH_{zpc}: ≈6.5 for bare Fe_3O_4.

Table 1. FTIR bands assignments of bare MNPs, coated MNP, MNP@β-CD, and polymer of β-CD MNP@P-CD reported in the literature.

Support/Coating	Wavenumber (cm^{-1})	Functional Group	Bond Type
Bare Fe_3O_4 MNP	3142–3500	O–H	H_2O adsorbed stretching vibration
	1000–1600	O–H	H_2O bending vibration
	400–700	Fe–O	asymmetric and symmetric stretching
$MNP@SiO_2$ and silane	1085–1100	Si–O–Si	asymmetric stretching of the oxygen bridge
	990	Si–O–H	stretching vibration of non-bridging oxygen in Si–OH or $Si–O^-$
	800–810	Si–O–Si	symmetric stretching of the oxygen bridge
	467	Si–O–Si	oxygen bending
MNP@MPS *	1712	C=O	ester groups on the surface from MPS
	1634	C=C	C=C from MPS
MNP@EPO **	2852–2934	CH_2, CH	stretching
$MNP@SiO_2@NH_2$ or $MNP@SiO_2$@PEI ***	3400–3420	N–H	symmetric and asymmetric stretching of the free NH_2 groups
	2865, 2930	CH_3, CH_2, CH	stretching
	1615–1630	N–H, C=N	bending scissoring mode of NH_2 Stretching from C=N
	1421	N=N	stretching of N=N from 5-amino-tetrazole
	875	N–H	bending, NH_2 and N–H wagging
MNP@CD or MNP@P-CD	3300–3500	O–H	stretching of the O–H, H_2O from CD or Fe_2O_3
	2865, 2930	CH_3, CH_2, CH	stretching of C–H
	2243	C≡N	stretching
	2115	Fe–C	stretching
	1994	Fe–CO	stretching
	1747–1685	C=O	carboxylic, ester and/or ketone stretching
	1629–1661	O–H	O–H bending
	1625–1640	N–H	NH_2 bending scissoring
	1623	COO–Fe	COOH asymmetric stretching
	1615	C=O	amide stretching
	1417–1460	CH_2, CH_3, O–H	CH_2, CH symmetric bending, scissoring O–H bending in plane
	1459	C–N	quaternary ammonium stretching
	1310–1380	CH	CH_2 asymmetric vibration and O–H bending
	1100–1265	C–O–C	C–O–C glycosidic stretching
	1020–1077	C–C/C–O	C–C and C–O stretching vibration
	937–947	R-1,4-bond	skeleton C–H vibration

* MPS = (3-methacryloxypropyl)trimethoxysilane, ** EPO = (3-glycidyloxypropyl)trimethoxy silane, *** PEI = polyethylenimine.

Table 2 provides a summary of the experimental methods and data used to characterize bare MNP, MNP coated with silica, silanes, amine, or β-CDs, MNP@CD, and polymer of β-CDs, MNP@P-CD.

Table 2. Different analytical strategies to characterize MNP and MNP@CD.

Method	MNP	MNP@CD or MNP@P-CD
XRD	2θ—planes 2θ = 30.2°, 35.6°, 43.2°, 53.7°, 57.2°, 62.9° (220) (311) (400) (422) (511) (440) Fe_3O_4 JCPDS card n°19-629 Fe_3O_4 JCPDS card n°88-315 Fe_3O_4 JCPDS card n°89-3854 Inverse cubic spinel magnetite belonging to space group Fd-3m	For 2θ = 18.8°, broad diffraction peak of β-CD
		No peaks (110) and (104) for 2θ = 21.228° or 33.158° No goethite (α-FeOOH) and hematite (α-Fe_2O_3)
		Broad featureless peak at low diffraction angle for amorphous SiO_2 shell
		No change in crystal phase of MNP@P-CD 12° to 26° broad peaks with amorphous polymeric layer
		With HP-β-CD, amorphous peaks in the range 10–15° and 15–25°
		Broad peak at 20–30° with polyurethane
XPS	Peak (eV) 714.08—Fe 2p divided into 727.9—Fe $2p_{1/2}$, 714.2—Fe $2p_{3/2}$ 529.36 O 1s 710.86—Fe 2p divided into 725.01—Fe $2p_{1/2}$, 711.5—Fe $2p_{3/2}$	Peak (eV) 284.8 C 1s divided into 288.9 C=O–O^- (carboxyl), 287.3 C=O (carbonyl) 531.8 O 1s divided into 536.8 O=C–O, 535.5 C–OH/C–O–C, 533.5 Fe–O–C
		New peaks at 400.3—N 1s, 689.88—F 1s 399.5 N 1s, N=N- at the surface
		401, 402 N 1s, ammonium functional groups
		From the ether bonds between lignin and β-CD 284.6 C 1s C–C/C=C/C–H From β-CD skeleton and lignin carbon ring structure 531.42 O 1s divided into 530.67 C=O, 531.9 C–OH/C–O–C, 284.69 C 1s C–C/C=C/C–H
TGA	<130–140 °C Weight loss: evaporation of residual water >130 °C sometimes weight gain: oxidation of Fe_3O_4 to Fe_2O_3. >200 °C loss of physically adsorbed OH groups or hydrogen-bonded water	<200 °C: weight loss of residual water adsorbed to the surface, caged inside β-CD cavities, and solvents 200–350 °C: weight loss of the linkage between MNP and β-CD 350–500 °C: weight loss of β-CD and polymer layer 690 °C: phase transition from Fe_3O_4 to FeO and deoxidation of FeO From the mass loss, the amount of β-CD anchored can be evaluated
Zeta potential	$pH_{zpc} \approx 6.5$	If pH < pH_{zpc}, surface charge is positive (protonation of MNPs, COOH groups, ammonium groups…) Favorable for adsorption of anionic dyes
		If pH > pH_{zpc}, surface charge is negative Favorable for adsorption of cationic dyes
VSM	Size less than 30 nm with zero coercivity and zero remanence exhibits superparamagnetism Magnetic hysteresis loop (type S-like)	Decrease of saturation magnetization due to non-magnetic materials at the surface When strong response to magnetic field, MNP@CD easily separated by an external magnet facilitating recoverability and reusability of the adsorbent after dye absorption
TEM/DLS	TEM in dried state DLS with water-swollen particles Values not comparable Particle size DLS > TEM	

There are two strategies to immobilize β-cyclodextrins or polymers of cyclodextrins on iron nanoparticles: the use of covalent or noncovalent bonding, as illustrated in Figure 6. The covalent routes require strong chemical reactions or conditions to substitute the hydroxyl groups on the surface of the material, such as with a silica coating, autoclave, plasma activations, or carboxylation reaction. The noncovalent route uses softer conditions and generates hydrogen bonding interactions between the entities.

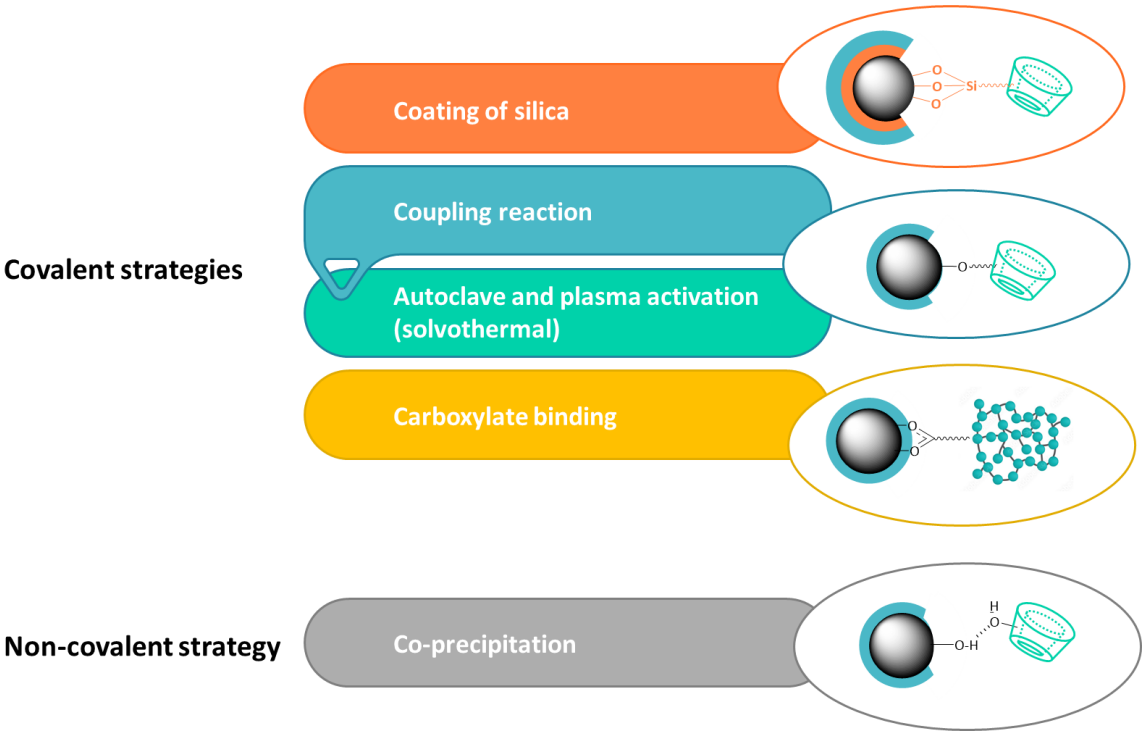

Figure 6. Different methods for β-CDs and polymer of β-CDs immobilization on MNP.

2.1. Covalent Strategies

2.1.1. Coating of Silica

The bonding between the Fe_3O_4 core and silane generates strong interactions and stable MNPs, which are particularly sensitive to extreme pH conditions. Indeed, at high acidic pH, MNPs tend to agglomerate and dissolve in the form of Fe^{2+}, Fe^{3+}, and oxonium ions [38]. The first layer is carried out following a method described by Stöber [50] in the presence of ethanol, an aqueous solution of ammonia, and the addition of tetraethyl orthosilicate ($Si(OC_2H_5)_4$), TEOS [43].

Under these condition reactions, TEOS is hydrolyzed into orthosilicic acid $Si(OH)_4$, which condenses onto the surface of iron nanoparticles bearing active hydroxyl functions, forming a protective layer of SiO_2 (Scheme 1). The TEOS being used in excess, some $Si(OH)_4$ molecules condense together, leading to single silica SiO_2 particles. This secondary reaction can be controlled by a slow addition of TEOS and washing treatments. Yilmaz et al. [51] first reported in 2013 the immobilization of cyclodextrin in one step from the MNP using a combination of TEOS reagent and a reactive synthesized 3-(2,3-epoxypropoxy)propyl]trimethoxysilylated β-CD (CD-$Si(OEt)_3$) (Table 3, Entry 1). The pure Fe_3O_4 MNPs were obtained by using a solution of Fe^{2+} and Fe^{3+} in the presence of sodium dodecyl sulfate in xylene and NH_3 reagent. The diameter of the particle slightly increased from 4 ± 2 nm for pure Fe_3O_4 to 7 ± 2 nm for MNP@CD. The spinel crystal structure and presence of aggregate were confirmed. Du et al. in 2015 [52] obtained a similar MNP@CD structure in two steps of synthesis, with firstly, the coating of Fe_3O_4 obtained by co-precipitation under hydrothermal conditions, with TEOS using the sol-gel Stöber method, followed by the grafting of CD-$Si(OEt)_3$ in the presence of ammonia (Table 3, Entry 1). The TEM image showed an evolution of the particle diameter from 10 nm to 250 nm with smoother surfaces, with a shell thickness of about 90 nm. The XRD pattern of MNP@TEOS core–shell nanoparticles revealed an amorphous state. The magnetic properties are reported, and superparamagnetism, low coercivity, and no hysteresis were observed. The saturation magnetization values for Fe_3O_4 nanoparticles and MNP@CD were 83.24 and 29.53 emu/g, respectively, validating the formation of the coating and possible magnetic solid/liquid separation. In 2016, Wang et al. [53] replaced the TEOS reagent by amino silane coating using (3-aminopropyl)triethoxysilane

(APTES), leading to a functionalized silica layer (Table 3, Entry 2). The reactive 6-O-toluenesulfonyl-β-cyclodextrin was added to get the magnetic nanocarrier. For each step, the thermogravimetric analysis was performed, leading to a loss of water, then a decomposition of the amino linker and CD (Figure 7a).

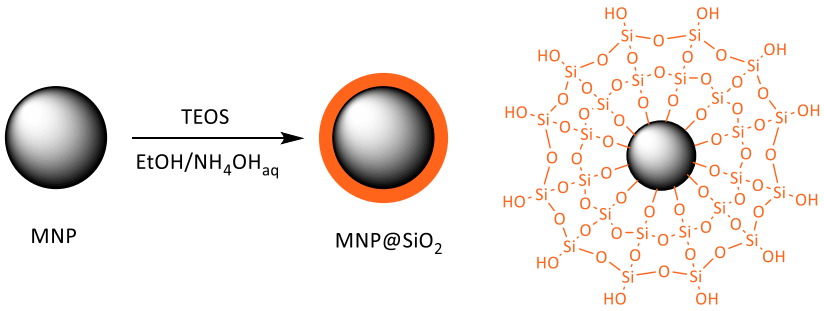

Scheme 1. Coating of silica using TEOS reagent on MNP.

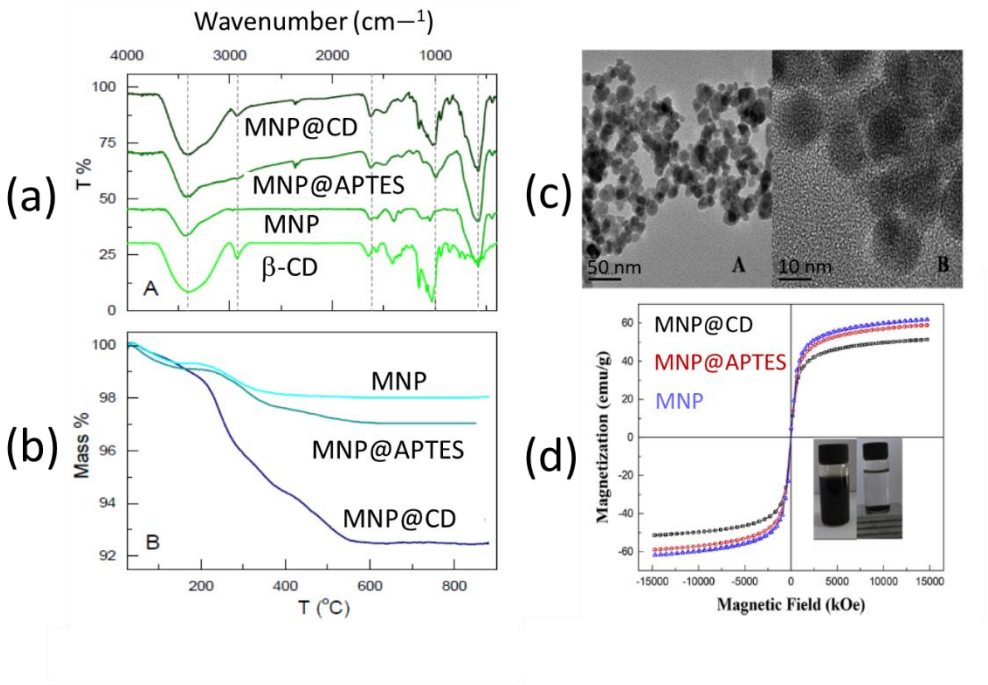

Figure 7. (**a**) FT-IR Spectra of β-CD, MNP, MNP@APTES, and MNP@CD; (**b**) TGA curves of MNP, MNP@APTES, MNP@CD; (**c**) TEM image of MNP (A) and of MNP@CD (B); (**d**) Magnetization curves of MNP, MNP@APTES, MNP@CD measured by vibrating sample magnetometer at room temperature; Pictures of MNP in the absence (**left**) and the presence (**right**) of an external magnetic field. Reproduced with permission from L. Wang, 2016 [53].

From the mass loss, the amount of β-CD anchored on the MNPs surface was estimated to be ~6 mass % corresponding to 60 mg/g of MNP. The hydrodynamic diameter of MNP@CD in aqueous solution, estimated at 56 nm was measured by transmission electron microscopy and dynamic Light Scattering (DLS), with each step increasing the thickness of the particles (Figure 7b). The functionalization did not modify the solid state. The magnetic properties were studied by a vibrating sample magnetometer as shown in Figure 7c. No hysteresis was observed with zero remanence, and coercivity indicated nanoparticles with a single domain. A decrease of the magnetization saturation value (Ms) of 62, 59, and 51 emu/g was observed with the increase of the layer thickness. Such a final value is still efficient enough to manage the magnetic solid/liquid separation. Interestingly, the authors reported an in vitro cytotoxicity study of MNP@CD on human hepatoblastoma HepG2 Cells and the viability observed proved the non-toxic effect of the functionalized nanoparticle. Another coating of MNP obtained by coprecipitation was reported in two steps

by Heidari in 2018 [54] (Table 3, Entry 3). Stöber's method was applied using 3-methacryloxypropyltrimethoxysilane (MPS) as a silane coupling agent to improve the stability and prevent the aggregation phenomena. The last step was a polymerization reaction between the immobilized acrylate function and a cyclodextrin acrylate and *N*-isopropylacrylamide as monomers, a radical initiator (AIBN), and *N,N*-methylenebis(acrylamide) as crosslinker. The thermoresponsive-magnetic molecularly imprinted polymer nanocomposite obtained was characterized using SEM, FT-IR, XRD, and TGA experiments. The presence of two ester and amide bands in FT-IR confirmed the successful polymerization onto the surface. The XRD patterns of the MNP@P-CD indicated the amorphous polymeric layer and an unchanged crystallography pattern. The thermogram profile showed the water elimination loss, the decomposition of the nanocomposite, and the reticulation linker. The morphology by SEM/EDS analysis revealed an evolution of the size of the MNP from 15 nm to 30 nm in thickness of the silica coating. The spherical final compound was reported to have a diameter of 130–150 nm. While the magnetic behavior was modified by the presence of the polymer around the iron core, and only 4 emu/g was measured, the author confirmed that the material could be easily dispersed with the help of an external magnet. Finally, the phase transition behavior of MNP@P-CD nanocomposite was studied by the dynamic light scattering (DLS) technique. A variation of the hydrodynamic diameter from 151 nm to 115 nm was observed at 34 °C due to a swelling process by water adsorption, hydrogen interactions, and conformation changes in the polymer. Aberoomand-Azar, in 2020, Ref. [55] reported a magnetic solid phase extraction based on poly(β-cyclodextrin-ester). Magnetic nanoparticles were obtained under pression using a Teflon lined stainless-steel autoclave in the presence of PEG and ethylene glycol (EG) and sodium acetate (ACNa) at 200 °C for 16 h (Table 3, Entry 4). A first coating was applied using TEOS reagent under basic conditions. The next functionalization occurred via the addition of (3-glycidyloxypropyl)trimethoxy silane (EPO), leading to epoxy reactive function ready to be grafted to a poly(β-cyclodextrin-ester) obtained from benzophenone tetracarboxylic dianhydride reagent. For each step, new FTIR bands were observed, such as the Fe–O band at 625–633 cm^{-1}, Si–O–Si stretching vibration at 1000–1100 cm^{-1} from silica coated Fe_3O_4, EPO C–H bond at 2852 and 2934 cm^{-1}, carbonyl groups of the ester and ketone groups of P-CD at 1656 and 1718 cm^{-1}. MNP@SiO_2@P-CD has a uniform size distribution and nearly spherical shape with an average size around 40–50 nm. At pH 5, the carboxylic groups of MNP-CDP, being ionized, interacted with the cationic dyes malachite green and crystal violet via electrostatic interactions. At low pH, hydrogen bonding interactions occurred between the nitrogen atom of the dyes and the carboxylic groups of the adsorbent. In addition, the formation of host-guest inclusion complexes also enhanced the extraction process.

Table 3. A summary of MNP@CDs prepared via a coating of silica.

Entry	Synthetic Scheme	Dye/Use	Ref.
1	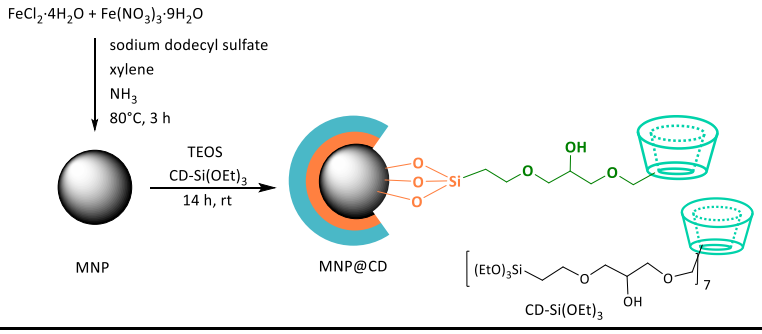	Direct blue 15 Evans blue Chicago sky blue	[51]
		Chemosensor of Cu^{2+} and other ions Host-guest inclusion complex with adamantane-modified salicylrhodamine B	[52]

2	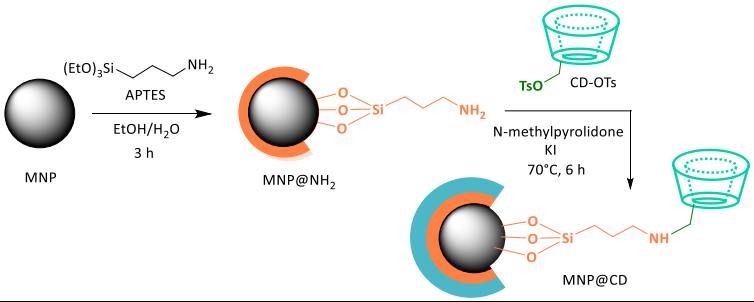	Methylene blue Adsorption pH 8 at 25 °C Desorption pH 7.4 at 37 °C	[53]
3	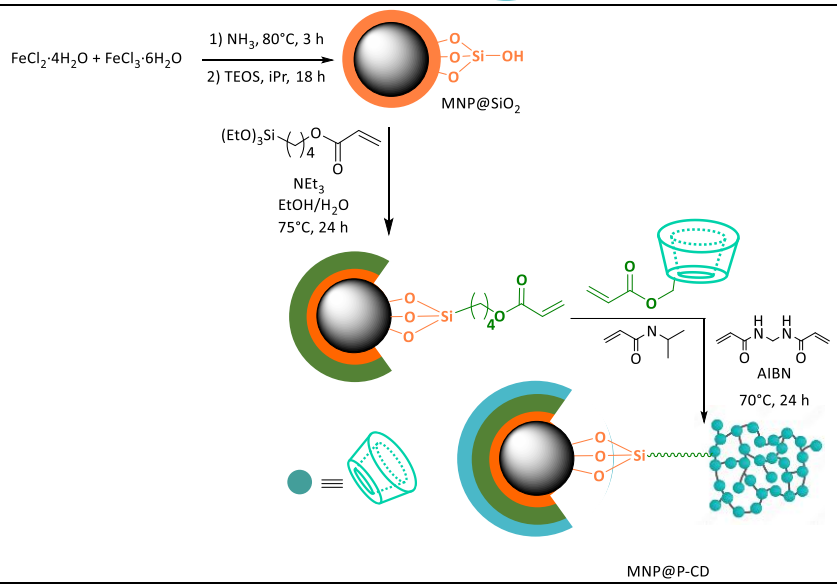	Curcumin Adsorption Methanol/acetic acid 9:1 Desorption pH 7.4 Phosphate buffer/DMSO 9:1 at 25 °C and 38 °C	[54]
4	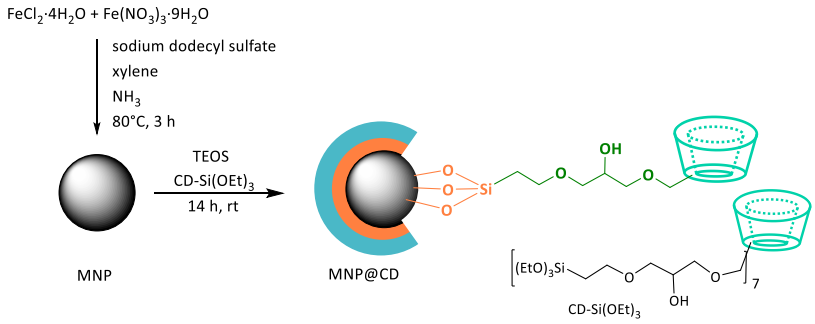	Malachite green Crystal violet Desorption Methanol-acetic acid (95:5 *v*/*v*)	[55]

2.1.2. Coupling Reactions

A maleic anhydride copolymer of β-CD was also immobilized on iron oxide nanoparticles by Jadeja et al., in 2019, Ref. [56] using coupling reagents such as *N,N′*-dicyclohexylcarbodiimide (DCC) and 4-dimethylaminopyridine (DMAP) as a catalyst (Table 4, Entry 1). The MNP was coated by the formation of ester covalent linkages between the hydroxyl groups on the Fe_3O_4 surface, which react with the acid carboxylic free function on the polymer of cyclodextrins P-CD. The XRD diffractogram proved that the incorporation of a polymer layer did not change the crystal phase of the particles. The high-resolution transmission electron microscopy (HR-TEM) images showed nanosized aggregates having a size range of 20−30 nm for the iron core. The layer of MNP@CD appeared as a light field contrast with spherical monodispersed particles with a size distribution of 50−60 nm. The performance of magnetic materials shows a decrease of magnetization of 10 emu/g. A specific surface area of 40 cm^2/g and total pore volume 14.96 cm^3/g were measured by BET analysis, whose isotherm shape belongs to type II among IUPAC classification, suggesting that these particles are mostly nonporous or macroporous and revealing possible physisorption or monolayer adsorption. In 2010, Uddin et al. [57] introduced covalently carboxymethyl-β-CD directly onto hydroxyl groups of iron nanoparticles, obtained from a chemical co-precipitation method

via carbodiimide (Table 4, Entry 2). The grafting was confirmed by FTIR with characteristic peaks at 945, 1030, 1157, and 1704 cm^{-1} and TGA (4.7 wt%). A mean diameter of 12 nm after β-CD immobilization and a hydrodynamic diameter of 28 nm were observed. The saturation magnetization value (Ms) decreased from 75 to 68 emu/g. The zeta potential study was performed at different pH. The isoelectric point (pI) shifted from 6.78 for the crude Fe_3O_4 to 5.9 for MNP@CD, meaning that the particle is positively charged at pH < 5.9. Two adsorbents with 4.7 wt% and 12 wt% in carboxymethyl-β-CD were tested for the adsorption of methylene blue. At pH 8 and 12, the support with the higher grafting rate adsorbed approximately twice as much of the dye. At low pH, methylene blue molecules compete with oxonium ions which generates low adsorption. Between pH 4 and 10, hydrophilic and hydrophobic groups are present in the dye, increasing adsorption.

Table 4. A summary of MNP-CDs prepared via coupling reactions.

Entry	Synthetic Scheme	Dye/Use	Ref.
1	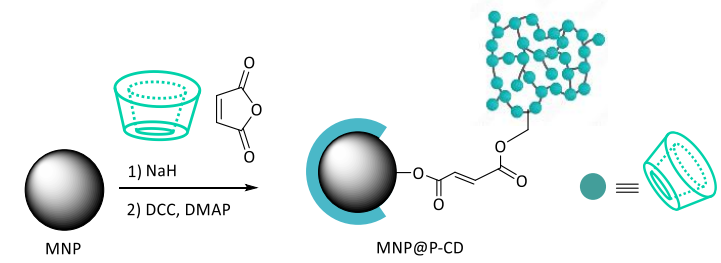	Malachite green Methylene blue Rhodamine 6G Desorption Ethanol-water 1:1 and water	[56]
2	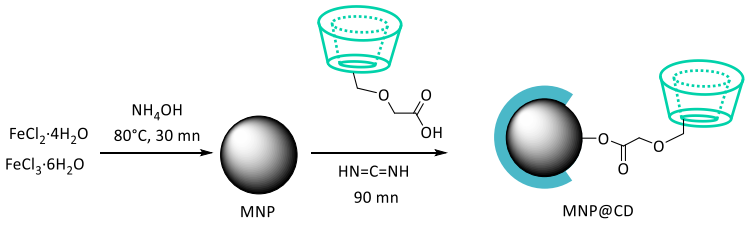	Methylene blue Desorption in methanol acetic acid (0–5%) or under acidic pH (<3)	[57]

2.1.3. Autoclave and Plasma Activations

Plasma treatment was used by Wang et al. [58] to graft CD onto MNPs by solvothermal technic based on the use of a stainless-steel autoclave at high pressure and temperature, in the presence of trisodium citrate, sodium acetate, and PEG (Table 5, Entry 1). Plasma activation is a green alternative to chemical strategy. However, various parameters have to be optimized to reach an efficient coating, such as the input N_2 gas to obtain the plasma state or the current strength of the voltage applied. The formation of highly reactive free radicals occurs, and rearrangement between hydroxyl functions on the cyclodextrin crown generates covalent and random bonds on the surface of the particle. Monodisperse uniform magnetic microspheres with a similar diameter of 200 nm and a similar crystal structure have been observed by TEM, SEM, and XRD before and after plasma treatment. No cyclodextrin layer was observed due to a low grafting rate of around 6.84% determined by TGA analysis. Moreover, a decrease in the saturation magnetization of the naked Fe_3O_4 particles occurred from 74.9 to 62.1 emu/g, attributed to the presence of the nonmagnetic β-CD coating, allowing the use of a low external magnetic field for the extraction step. The specific surface areas were enhanced from 18.84 to 25.67 m^2/g. The zeta potential study in function of surface pH showed that the isoelectric point (IEP) drastically shifted from 6.6 to 3.9, indicating a positively charged particle at this pH. The adsorption of naphthylamine was tested on three MNP@CD containing 2.50% wt, 6.84% wt, and 9.32% wt of β-CD at pH 6.5. The adsorption capacities increased as the content of β-CD increases. The adsorption of 1-naphthylamine is dependent on pH, the mechanism being a compromise between electrostatic and hydrophobic interactions with the surface. In 2019, Pan et al. [59] introduced a

polyethyleneimine bi-functionalized magnetic nanoadsorbent using an optimized solvothermal method in a teflon-lined autoclave in the presence of a diamine (Table 5, Entry 2). Polyethylenimine (PEI) is a water-soluble polymer that can chelate cationic metals thanks to its amino groups and anionic pollutants at acidic pH conditions. The combination between PEI and CD reinforces its capture properties. PEI was immobilized via imine functions by addition of glutaraldehyde crosslinker. The final nanohybrid particle was obtained using 6-monosuccinyl-β-CD in the presence of amidation coupling reagents. The various steps were followed by FT-IR experiments, and a strong peak at around 1640 cm^{-1} was attributed to characteristic amide function absorption. No aggregation was observed by SEM. PEI coating increased the size of the particles from 50 to 150 nm, but the presence of CD did not result in any structural change. The saturation magnetization value decreased from 81.3 for the crude MNP to 60.3 emu/g for the hybrid bicomposite, respectively. The introduction of CD on MNP@PEI generates a decrease in BET from 19.787 to 17.514 m^2/g. Finally, TGA curves could be interpreted into four reaction steps for all the samples. A weight loss of about 3.5 wt% observed by thermal decomposition for MNP@PEI@CD is evidence of the presence of covalent links between MNP and the macrocycle. The authors concluded that electrostatic attraction between positively charged amino groups of PEI and negatively charged sulfonate of methyl orange played a dominant role in the uptake of this dye by the adsorbent in a broad pH range. Effectively, at pH 6–9, the low surface adsorption via electrostatic interactions is compensated by host-guest complex formation, resulting in a constant adsorption in this pH range. In addition, hydrogen bond interactions between hydroxyl groups of β-CD and the dye were also involved in the uptake process. The same year Zhou et al. [60] described the synthesis of magnetic nanospheres functionalized by β-cyclodextrin polymer. The direct solvothermal method was applied to obtain MNP@CD from $FeCl_3$ in the presence of sodium acetate and ethylene glycol solution and β-CD (Table 5, Entry 3). A second autoclave reaction was performed using tetrafluoroterephthalonitrile monomer and carboxymethyl-β-CD under hydrothermal conditions reaction. The high temperature and high pressure applied improve the radical polymerization reaction, which occurs via nucleophilic aromatic substitution of the fluorine on the benzene ring by the hydroxyl groups of the macrocycles. Both monomer and cyclodextrin play a role in the remediation strategy. The MNP@P-CD can be observed as a uniformly spherical porous morphology surface by SEM. The thickness of the layer was estimated to be around 20 nm after the polymerization reaction. The presence of Fe, C, N, O, and F atoms was quantified by HAADF-STEM and confirms the final structure. The spinel structure of the magnetic core remains stable after the autoclave treatment. In IR spectra, the cyanoaromatic groups exhibit absorbance at 1648 and 1443 cm^{-1} and the C–F stretching vibration at 1267 cm^{-1}. The thermogravimetric analysis of the nanospheres showed a weight loss of 8.6% of the initial weight, attributed to the grafting of β-CD, and a loss of 28.5%, assigned to the polymer coating. Polymerization has a greater impact on the material's magnetic properties. Indeed, the Ms decreases from 70.2 to 44.8 emu/g. Consequently, the MNP@P-CD can be segregated from the solution under an external magnetic field after several minutes. XPS spectra revealed the presence of a carboxylate peak at 288.9 eV and Fe–O–C peak 533.5 eV illustrating the interaction between the carboxymethyl-β-CD polymer and the hydroxyl group of the surface of the metal. Finally, BET characterization and N_2 adsorption desorption isotherms showed a surface area of 44.44 and 70.63 m^2/g, for MNP@CD and MNP@P-CD, respectively; a larger surface meaning larger adsorption capacity. The pore size was estimated at 5.59 nm, large enough to encapsulate an organic pollutant. The adsorption mechanism of methylene blue on MNP@P-CD is summarized by the authors in a well-described scheme with host-guest complex interaction, hydrogen bonding, and π-π interactions. In 2025, Bakshi et al. [61] functionalized iron oxide nanoparticles with β-CD using surfactants to enhance the interactions on the interface solid/liquid by self-association (Table 5, Entry 4). Two polar chains were tested hexamethylenebis(hexadecyldimethylammonium bromide) (16–6–16) and tris(2-(*N*-dodecyl *N,N*-dimethylammonio)ethylamine)tribromide (TriCAT). Hydrothermal method was performed in presence of β-CD and surfactants. Ionic interactions and covalent bonding occur between the iron core and

hydroxyl functions of the macrocycle and the positive charges of the surfactant, respectively. The authors have studied the adsorption of many aromatic dyes and have underlined the presence of van der Waals-like attractive forces between the dye molecules, leading to self-association and reducing host–guest interactions with the CD cavities. Consequently, the extraction of dyes is low in neutral water, when the self-association is at a maximum. Adsorption is highly facilitated at highly acidic and/or basic pH. Under these conditions, an ionization of the dye molecules occurs, generating a surface activity which drives a solid-liquid interfacial adsorption on MNP. At the interface, the aromatic moieties of the dye molecule find the CD cavity as an ideal host providing anchoring and extraction.

Table 5. A summary of MNP-CDs prepared via autoclave and plasma activations.

Entry	Synthetic Scheme	Dye/Use	Ref.
1	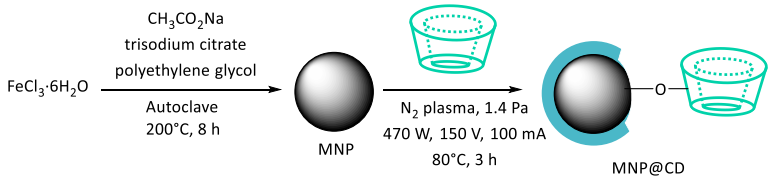	Metal ions Cu(II) 1-naphtylamine	[58]
2	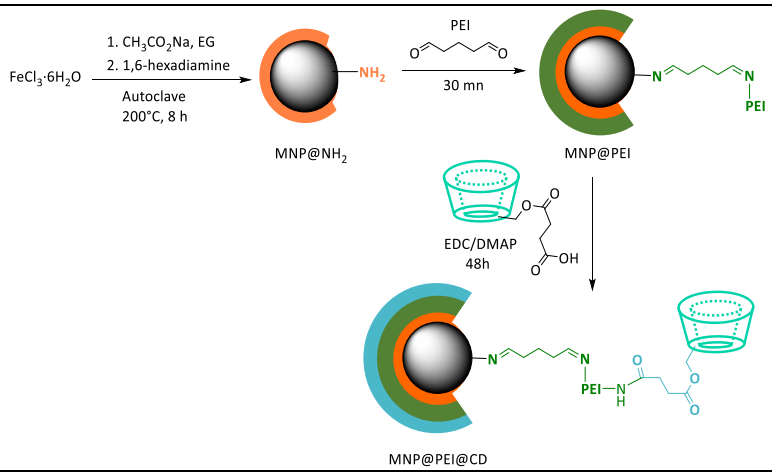	Methyl orange Pb(II) Desorption in basic and acidic pH, methanol	[59]
3	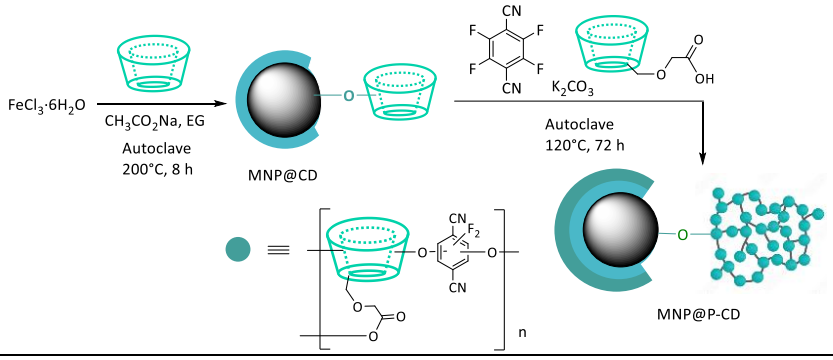	Methylene blue Absorption pH: 3–11 Desorption ethanol solution containing 5% (*v*/*v*) acetic acid	[60]
4	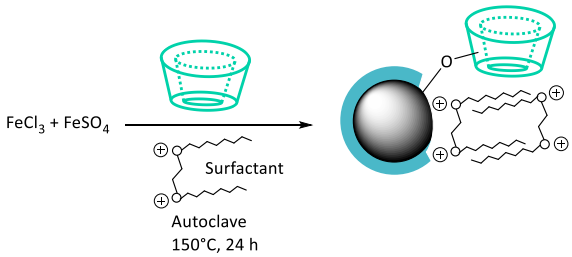	Red 40 Yellow 5 Yellow 6 Blue 1	[61]

2.1.4. Carboxylate Bonding

Many MNP@CD composites are based on the use of carboxymethyl-β-cyclodextrin using the chemical co-precipitation method [62] (Table 6, Entry 1). The properties of magnetic nanoparticles were measured using powder X-ray diffraction (PXRD), zeta potential analysis, and magnetization measurements. BET experiments revealed specific surface areas of 64.5 and 60.4 m^2/g for Fe_3O_4 and coated MNP, respectively, with the same crystalline phase structure. Zero-point charge values decrease for the composite (4.0 *vs*. 6.5) due to the presence of hydroxyl and carboxymethyl function. In the same way, the saturation magnetization values change from 75.0 to 56.5 emu/g, respectively, which correspond to a mass fraction of 24.6% cyclodextrins. A stability study was performed in the pH range of 2–10. At pH 2, a higher Fe atom is released in the absence of coating (35%), and no release is observed at pH 8. For MNP@CD the proportion of leached Fe is 4% at pH 2.0 to zero at pH 6.0. Consequently, the layer of CD improves the pH stability of the particles. Basic blue 3 (cationic dye) adsorption studies on magnetic materials suggest that chemisorption rather than diffusion was the predominant driving force. Faramarzi et al. [63] in 2017 developed a magnetic β-cyclodextrin-anhydride polymer nano-adsorbent (Table 6, Entry 2). An iron oxide core was prepared using the co-precipitation method in an alkaline medium. A polymerization reaction occurred with β-CD using succinic and dicarboxylic anhydrides (Epiclon B-4400) in the presence of NaH. The link between the MNP and the polymer is based on a bidentate complex between the iron metal and the carboxylate function formed after opening of the anhydride cycles. The adsorbents were characterized by FTIR, XRD, SEM, TGA, and VSM analysis. A characteristic band at 1740 cm^{-1} is assigned to the C=O asymmetric stretching vibration of the ester groups proving the presence of polymer structure. The synthesized MNP@P-CD retained the Fe_3O_4 spinel structure and had a uniform size and shape, with a diameter of around 40 nm. At each step, the saturation magnetization decreases from 69, 38, and 20 emu/g attesting the presence of non-magnetic coating. TGA and FTIR analysis confirmed the successful synthesis. A weight loss of 2.5% within the temperature range from 200 to 450 °C was related to decomposition of β-CD layer corresponding to 2.5–10 wt%. The surface charge was altered at the isoelectric pH of 5.6, indicating the presence of a positive charge at this pH. Consequently, alkaline conditions will favor the adsorption of cationic dyes. In this work, the authors propose two mechanisms responsible for dye adsorption: electrostatic attraction and host-guest inclusion complex formation. For the rhodamine B, the dominant mechanism could be the electrostatic attraction of the positively charged dye molecules and the negative sites of the adsorbent (e.g., hydroxyl groups), which was confirmed by a pH study. Nevertheless, rhodamine B has a bigger size than methylene blue and cannot be included into the β-CD cavity. The same year, Luo et al. [64] immobilized cationic polymer of β-cyclodextrin on magnetic nanoparticles as nano-adsorbents from β-CD, succinic anhydride, and 2,3-glycidyltrimethylammonium chloride (Table 6, Entry 3). MNP was synthesized by co-precipitation, with an excess of ammonia at pH 10–11. The reaction occurred in two steps, the first is the ring opening polymerization of anhydride and β-CD via esterification reaction. Then, the addition of ammonium epoxide under basic conditions leads to etherification of the hydroxyl of the macrocycle. The residual acid carboxylic functions interact with hydroxyl groups, enrobing the surface of the iron core and forming a cross linked organic layer. FTIR, X-ray diffraction, contact angle, SEM, BET, VSM, and zeta potential analysis were performed to confirm the modified structure. In infrared spectra, the stretching vibration peaks at 1459 cm^{-1} and 1710 cm^{-1} related to C–N and C=O bands, confirmed the presence of crosslinker. The peaks at 1623 and 1401 cm^{-1} attest the formation of carboxylate-Fe binding. The XRD experiment confirmed the stable single-phase cubic-structure of Fe_3O_4 after functionalization with crystal diameters of the MNP and MNP@P-CD of 24 nm and 66 nm, respectively, decreasing the high surface energy of the MNP, and enhancing the dispersion properties due to the adsorption of the polymer into the active sites of the MNP. For this purpose, a contact angle solid/liquid experiment was performed to study the wettability and the free energy of the solid surface. This result (less

than 90°) indicated that the MNP@P-CD has a hydrophilic surface and would be dispersed in dyes solution. VSM analysis indicated a decrease in magnetization strength from 62.3 to 54.7 emu/g. This strong magnetism property allows for an excellent separation phase process. The isoelectric point of the MNP@P-CD was calculated at 7.48. Consequently, at lower pH, a protonation of the acid and amino functions will occur. In 2020, other composite was obtained using tetrafluoroterephthalonitrile cross-linked β-cyclodextrin previously obtained by polymerization and carboxylation reactions (Table 6, Entry 4) [65]. The formation of the Fe_3O_4 core was performed in situ by co-precipitation in the presence of polymers of cyclodextrins under basic conditions. The iron core was coated by the carboxylate functions. Here again, the synergistic effect of the presence of CD cavity, π-stacking and ionic interactions enhanced the adsorption properties. The strategy aims to increase the number of carboxylate sites to enhance the interaction with the metallic nanoparticles and to endow a negative charge surface to absorb cationic dye. The decrease of BET surface area highlights that the polymer of CD obstructs the iron nanopore. The SEM and 2D EDS mapping studies measured a ratio of 0.6Fe-0.96β-CD, and poorer crystal structures were observed. The XPS experiment confirmed the presence of many carboxylate groups due to the existence of Na peak. The zeta potentials of the polymer of CD and MNP@P-CD were determined at −30.8 and −27.6 mV, respectively, proving the presence of anionic groups and illustrating the influence of the iron core. The layer of nonmagnetic polymer decreases the magnetic properties of the MNP@P-CD as 92 *vs*. 16.6 emu/g was measured. Li et al. published, in 2020 [66], a green synthesis of a magnetic β-cyclodextrin polymer for rapid removal of organic micro-pollutants and heavy metals from dyeing wastewater (Table 6, Entry 5). The composite with many macro- and ultramicropores in the aqueous phase was obtained from a carboxymethylated β-CD-based polymer, which was obtained by polymerization reaction using epichlorohydrin, and tetrafluoroterephthalonitrile used as flexible and rigid crosslinker, respectively. The MNP@P-CD was synthesized in one pot by the co-precipitation method from iron salts in an ammonia medium by forming a strong bonding between the carboxylate ligand and the iron metal. Such interaction was observed in the FTIR spectrum with an absorbance at 1684 cm^{-1} related to C=O stretch vibration, in parallel, the characteristic band of Fe–O at 586 cm^{-1} of Fe_3O_4 shifted to 582 cm^{-1} after coating. Similarly, the XRD spectrum of the MNP@P-CD remains the cubic spinel structure of the Fe_3O_4 with a saturation magnetic susceptibility at 53 emu/g. Consequently, a quick aggregation phenomenon can occur, facilitating the phase separation under an external magnetic field. From the thermal mass loss experiment, the content of the organic layer was estimated at 20.37%, and the isoelectric point decreases from pH = 6.8 for the iron oxide precursor to 4.37 for the embedding MNP, attesting to the presence of negatively charged carboxyl groups on the surface. Sorption of bisphenol A, basic orange 2, rhodamine B, and methylene blue on the MNP@P-CD support was dominated by chemisorption. For bisphenol A, an inclusion complex may be formed with a cyclodextrin cavity, while the adsorption of rhodamine B and methylene blue may be related to the electronegativity of the –COOH groups on the surface of the magnetic support. The adsorption of basic orange 2 is based on the hydrophobic cavity and the –COOH group electronegativity of MNP@P-CD. Sun et al. reported recyclable magnetic microspheres obtained from ionic MNP in basic conditions in presence of β-CD, epichlorhydrin monomer (EPI), non ionic surfactant sorbitan monooleate (Span 89), and another detergent (Tween 20 Kerosene) (Table 6, Entry 6) [67]. The authors reported that basic fuchsin adsorption isotherms were indicative of chemisorption, reflecting strong electrostatic interactions between the cationic dye and the MNP@CD. The iron core was synthesized by co-precipitation of sodium citrate, leading to carboxylate charges on the surface of the nanoparticles. Thus, the synergic cationic interactions and formation of host-guest inclusion complexes improved the pollutant capture strategy. The structure and morphology were studied by FT-IR, XRD, SEM. In XRD patterns, a broad diffraction peak of the macrocycle appears near 18.8°. SEM images show spherical particles of uniform size with a particle size of about 45 μm. In 2023, Akbari et al. [68] published an easily recoverable nanoadsorbent based on *N*-heterocyclic copper(II) complex immobilized on the β-cyclodextrin-modified Fe_3O_4 nanoparticles (Table

6, Entry 7). This hybrid material was used for the catalytic reduction of toxic dyes in wastewater via wet-chemical method. The Fe_3O_4 nanoparticles was obtained using Fe^{2+} and Fe^{3+} under microwaves activation. A polymer of carboxymethyl-β-CD has been produced using epichlorydrin cross linker. The MNP was embedded under basic conditions with the CD-polymer, and the metallic surface was coated by the addition of (3-chloropropyl)trimethoxysilane. Then, 5-amino-1-tetrazole was introduced by nucleophilic substitution, and the copper ion was chelated by the immobilized aromatic ligand. Several characterization techniques including FT-IR, TGA analysis, FE-SEM/EDX, TEM, X-Ray diffraction patterns (XRD) measurements, were employed to investigate the structural properties of the synthesized material. The stretching vibration of N=N bonds was observed at 1421 cm^{-1}. The structure of cubic spinel in Fe_3O_4 and the crystal planes in Cu with homogeneous spherical core–shell distribution were confirmed. An EDX mapping element confirmed the presence of Cu atom with 5.24% of weight. The saturation magnetization value was determined at 16 emu/g due to the coating of polymer of CD around the iron oxide Fe_3O_4 nanoparticles initially at 92 emu/g. Multistep endothermic thermal decompositions were observed by TGA within 250–850 °C, attributable to organic components on the surface. Quaternary ammonium groups immobilized on porous magnetic cyclodextrin polymers was synthesized in 2023 by Cheng et al. [69] to adsorb anionic dyes (Table 6, Entry 8). The iron core was coated with sodium citrate via autoclave activation, leading to strong interactions between carboxylate, alcohol, and hydroxyl groups on the metal surface. Copolymerization occurred between perfluorodicyanobenzene monomer, β-CD and functionalized MNP generated a embedding layer. In a second step, the secondary alcohol function at O_2 position of β-CD crown was substituted by two quaternary ammonium propyloxy moieties with methyl and hexadecyl carbon chains, respectively. A positively charged final material MNP@P-CD@NR_3^+ was obtained enhancing the adsorption capacity through ionic interactions and host-guest complexation mechanisms. Moreover, ammonium groups bearing long carbon chains (C16) generate antibacterial properties due to interactions with the hydrophilic membranes leading to cells apoptosis. The experiment was performed on *Staphylococcus aureus* in water, and the efficiency was demonstrated. Peaks corresponding to CD and aromatic functions were assigned by infrared spectra. Ammonium C–N stretching vibration appeared at 1678 cm^{-1} and the CH_2 tensile vibration of the hexadecyl chain at 2923 cm^{-1}. The thermogravimetric analysis indicated that the final MNP maintains its thermal stability up to 270 °C with a faster mass loss for the quaternary ammonium surface-modified. The cyclodextrin content reported was 17.348%, 17.472%, and 25.447% for MNP@P-CD, MNP@PCD@NR_3^+ with short and long chains, respectively. Negative potential was observed for MNP@P-CD, and the positive charged was confirmed in the presence of ammonium salt. The low saturation magnetization values of 13.76 and 15.17 emu/g were reported for short and long ammonium chains, respectively. The particles were spherical with diameters of 200 to 600 nm and specific surface areas calculated for MNP@P-CD and short and long ammonium chains, respectively, were estimated at 107.482, 31.759, and 9676 m^2/g, respectively, with average pore diameters at 4679, 5736, and 9146 nm. The adsorption capacity of two anionic dyes was studied: orange G and methylene blue. The introduction of quaternary ammonium generates a positively charged support, favoring electrostatic interactions that are combined with host-guest interactions within the β-CD cavity. In addition, the introduction of hexadecyl chains further produce hydrophobic interactions as observed in the case of bisphenol A adsorption, a neutral dye. In 2025, Arami-Niya et al. [70,71] reported two publications in which they described the fabrication of β-cyclodextrin/magnetic lignin adsorbents using carboxylic acids cross-linkers (Table 6, Entry 9). The iron chloride hexahydrate and iron sulfate heptahydrate were treated with lignin in presence of ammonia solution (28 wt%). The phenolic groups of lignin interact with hydroxyl groups of ion core leading to a green coating. The β-cyclodextrin were immobilized on the magnetic nanoparticles thanks to an esterification reaction with carboxylic acids in excess of potassium dihydrogen phosphate. Three biobased crosslinkers were tested citric, tartaric, and malic acids to study the influence of geometry and the steric hindrance of the reagents on the capture efficiency of the final network magnetic

polymer. Indeed, the use of polycarboxylic reagents form high stable cross-linking networks with multiple reactive sites. The strategy aimed to combine cyclodextrin/kraft lignin/carboxylic acid moieties to enhance aromatic dyes magnetic extraction rate thanks to host-guest complexation, π-π stacking, electrostatic interactions, and hydrogen bonding. The adsorbents were characterized using various analytical techniques, including X-ray diffraction (XRD), Fourier transform infrared spectroscopy (FTIR), field-emission scanning electron microscopy (FESEM), and a vibrating sample magnetometer (VSM). A face-centered cubic structure was analyzed by XRD, indicating an unchanged crystalline structure of iron after esterification reaction with crystallite sizes between 4.11 to 10.72 nm. The presence of β-CD and lignin was confirmed with characteristic of stretching vibrations of C–C bonds at 1635 cm^{-1} and of vibrations of the benzene ring at 1594 cm^{-1}. Absorption bands around 1742/1747 cm^{-1} of the C=O stretching vibration attest that the carboxylic acid groups have formed ester bonds with the hydroxyl functions of β-CD and MNP@Lignin. The diameters of the particles decrease from 37.53 to 22.68 nm for the MNP@Lignin and MNP@Lignin@P-CD, respectively, with unchanged morphology. The initial spherical shape of the iron core is conserved after functionalization. However, the saturation magnetizations were measured at 2.52, 3.78, and 8.43 emu/g for citric, tartaric, and maleic acids, respectively. A thicker nonmagnetic coating generates lower magnetic performance by increasing the dipole moment. Consequently, citric acid crosslinker generates deeper and less accessible carbon networks. Similar zeta potential profiles with negative charges for a pH range of 3–11 were observed, with the most negative zeta potential for tartric acid, attesting higher content of carboxylate function on the surface. The SEM image confirms the lower porosity of the final nanoparticles. However, the interactions with the pollutants are only based on interactions with the organic function on the surface of the adsorbent. The suggested interactions involved in the adsorption mechanism and the related FTIR bands modifications observed are illustrated in Figure 8.

Table 6. A summary of MNP-CDs prepared via carboxylate bonding.

Entry	Synthetic Scheme	Dye/Use	Ref.
1	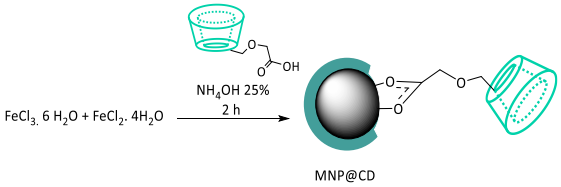	Basic blue 3 Desorption Solution containing acetic acid (5% *v*/*v*)	[62]
2	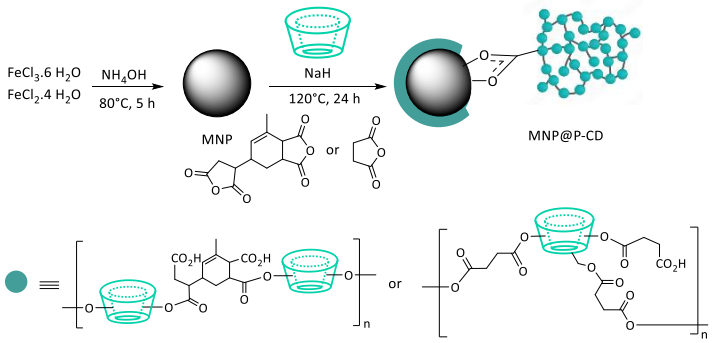	Rhodamine B Methylene blue Desorption Methanol, ethanol, acetic acid, methanol/acetic acid (9:1 *v*/*v*)	[63]

3	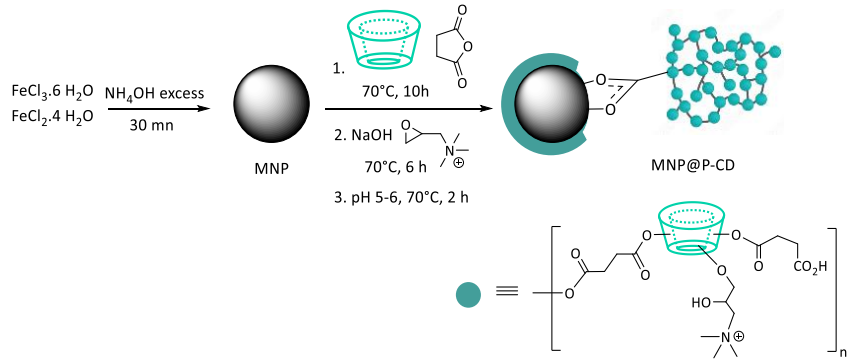	Congo red Cr(VI) Desorption in 1 M NaOH	[64]
4	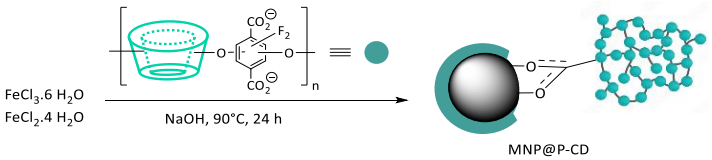	Methylene blue Methyl orange	[65]
5	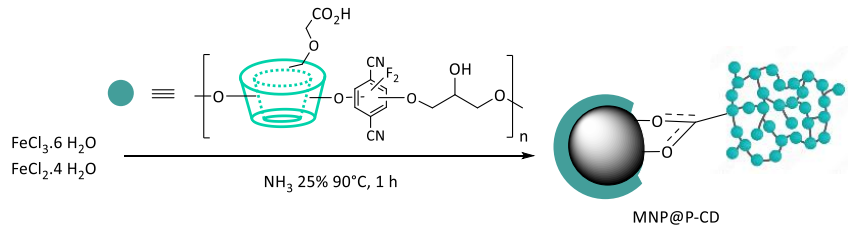	Bisphenol A Basic orange 2 Rhodamine B Methylene blue Heavy metals Cr(III), Pb(II), Zn(II), Cu(II) Desorption Methanol 5% acetic acid	[66]
6	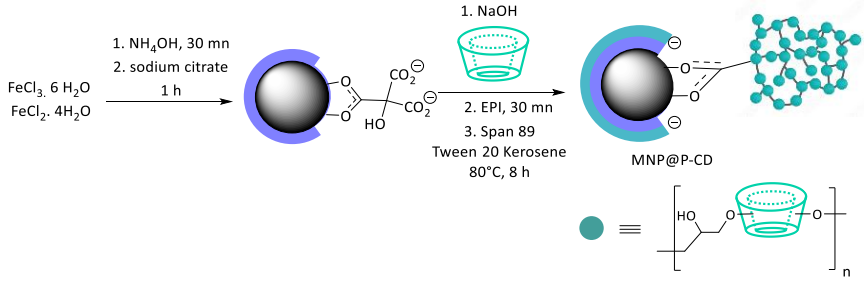	Basic fuchsin Desorption by HCl	[67]
7	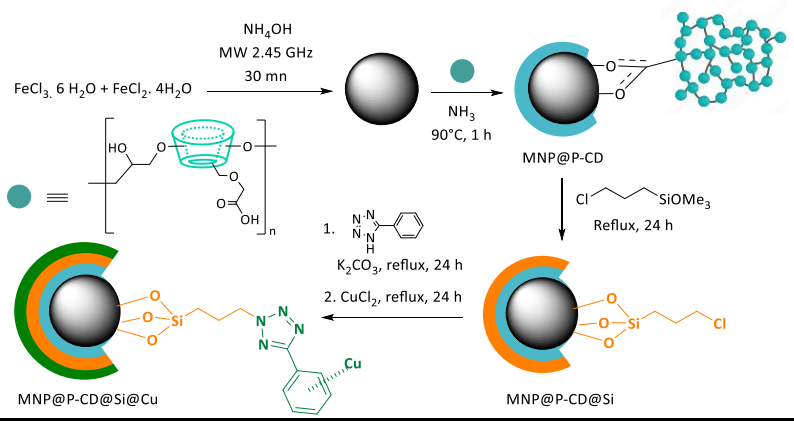	Catalytic reduction of p-Nitrophenol Eosin Y Rhodamine B Congo red	[68]

8	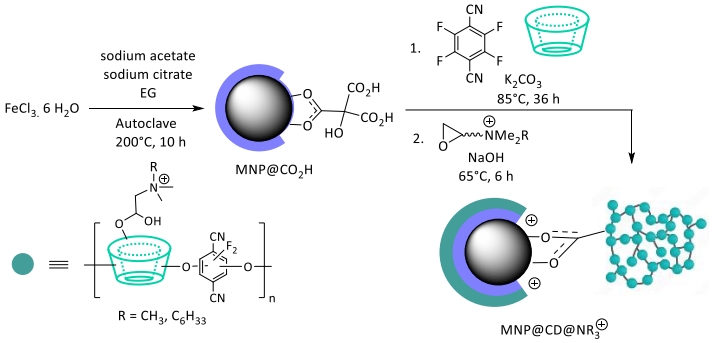	Methyl blue Orange G Bisphenol A Desorption 0.1 M NaOH, ethanol	[69]
9	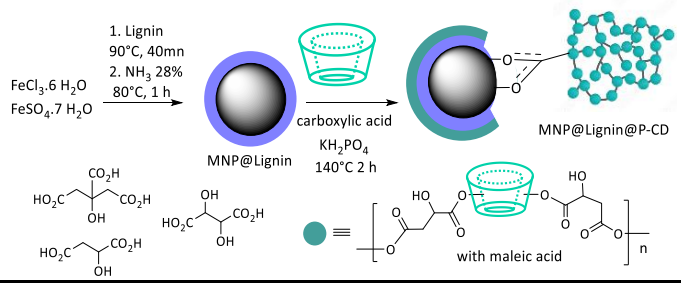	Methylene blue Desorption Ethanol/0.1 M HCl 3:1 for 30 min	[70,71]

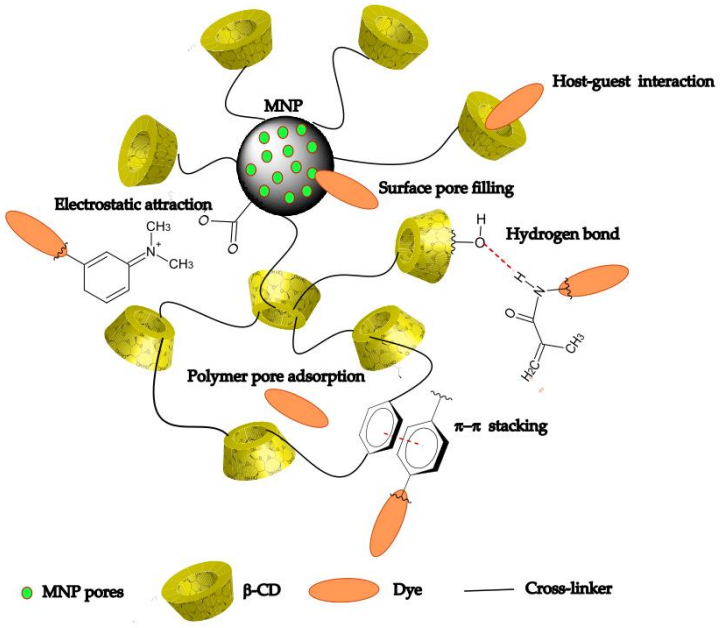

Figure 8. Interactions between MNP, β-CD, and dyes.

2.2. Noncovalent Strategy: Co-Precipitation Method

Al-Maddhagi et al. recently provided a mini review on the synthesis of MNPs using the coprecipitation approach, but not involving cyclodextrins [72]. In 2012, Sun et al. [73] grafted cyclodextrin–chitosan onto magnetic nanoparticles to nano-adsorb methyl blue (Table 7, Entry 1). In the presence of non-ionic surfactant (span 80) and liquid paraffin, glutaraldehyde was used as a cross-linker to improve the chemical stability in acid media, despite the fact that this polymerization step would reduce the amino chelating sites on the nanoparticles and consequently the adsorption capacity. However, the interactions with multiple hydroxyls, carboxyl groups, and free amino groups of the chitosan biomaterial and the formation of host–guest supramolecular complexes between the organic dye and the CD cavity still remained to reach a good remediation rate. SEM and TEM experiments showed spherical shaped particle morphology with diameters around 100 nm. The immobilization of CD-chitosan was confirmed by IR with characteristic peaks at 1650

cm^{-1} (CN stretching vibration). In 2016, An et al. [74] associated a carbonized rice husk (CRH) matrix with β-CD and Fe_3O_4, leading to an integrated multifunctional bioadsorbent (Table 7, Entry 2). The authors observed that the mixture of CRH with iron oxide reduced the adsorption capacity of the nanoparticles. To avoid this difficulty, they inserted CD using hydrothermal co-precipitation technique in three steps. β-CD was firstly stirred in presence of CRH and $FeCl_3$, then $FeCl_2$ was added, followed by $NH_3 \cdot H_2O$. The authors confirmed the creation of covalent bonding between hydroxyl functions of the β-CD and oxygen groups on the surface of the carbonized rice husk by reaction under alkaline conditions. This claim was based on ^{13}C NMR experiment in the absence of iron metal. Indeed, a new weak peak at 72 ppm was attributed to C–O–C interaction between the two entities. The surface of CRH@MNP@CD appeared rougher. The powder XRD technique showed very low peak intensities, indicating a low amount of iron nanoparticles (9.52% determined by XPS). EDX mapping suggested that Fe was evenly distributed in the composite with a low saturation magnetization of 6.5 emu/g. Increasing the pH of the system significantly enhances methylene blue adsorption capacity, mainly due to favored electrostatic attractions and hydrogen bonding between the cationic dye and multiple adsorptive sites, e.g., the hosting cavity, the hydroxyl groups of the CD crown, and surface oxygen-containing groups from the solution-carbonized matrices. After the adsorption step, the spectrum of CRH@MNP@CD shows distinct absorption changes at 1598, 1245, and 883 cm^{-1}, characteristic of the aromatic ring stretching vibration of methylene blue. A polymer of β-CD functionalized with ionic liquids was immobilized onto Fe_3O_4 to measure the rhodamine B in food samples by magnetic solid phase extraction (MSPE) (Table 7, Entry 3). FTIR data certified that the hydroxyl part of rhodamine B was included in the CD cavity [75]. Ionic liquids (ILs) are stable organic salts with hydrophobic properties. Mono-6-deoxy-6-(1-ethyl-imidazolium)-β-cyclodextrin iodide polymer was added to Fe_3O_4 nanoparticles in the presence of Fe^{3+} in basic conditions. The presence of modified cyclodextrin onto iron nanoparticles was confirmed with peaks of 1118 cm^{-1} and 1326 cm^{-1} corresponding to amide function, and C=O bond at 3127 cm^{-1}. The microscopic morphological structures revealed a layer shape and macropores different from the initial polymer. The crystal shape of Fe_3O_4 particles was not altered after the modification. Parashara et al., in 2018, Ref. [76] synthesized modified magnetic nanoparticles with β-CD by a simple co-precipitation method in a single step by mixing an aqueous solution of Fe^{2+}, Fe^{3+}, and ammonia (25 wt%) under heating at 70 °C for 30 min (Table 7, Entry 4). Spherical shape of nanoparticles with an average size of the nanoparticles at 8.6 nm was observed, and the TGA data support the formation of β-cyclodextrin modified MNPs. The interactions between the hydroxyl groups of the oligosaccharide crown and the carboxylate and phenolate groups of eosin and phloxine stabilize the dye encapsulation. The capture properties of hydroxypropyl-β-cyclodextrin-polyurethane magnetic nanoconjugates MNP@PU@CD were studied by Alizadeh et al. [77] (Table 7, Entry 5). They played with the dual absorbent properties of the macrocycle and urethane network to remove dyes. Hydroxypropyl β-CD (HP-β-CD) was tested due to its higher water solubility compared to β-CD. PU brings mechanical properties and water resistance to the composite. The authors compared the nanocomposite with and without PU. The iron nanoparticles were heated in the presence of HP-β-CD, leading to a noncovalent bonding. Covalent conjugation was achieved after polymerization of hexamethylendiisocyanate (HDMI) with Fe_3O_4 particles prepared from $FeCl_3 \cdot 6H_2O$ in an autoclave for 8 h at 200 °C in the presence of PEG 6000, sodium acetate, and ethylene glycol. Magnetic nanocomposites were characterized by FTIR spectroscopy. The absorption bonds of HP-β-CD and PU were recovered with the presence of stretching vibrations of NH–CO (1570 cm^{-1}), C–N (1253 cm^{-1}), only the Fe–O vibration moved from 573 cm^{-1} to 604 cm^{-1}. By SEM, the final nanoparticles appeared aggregated. In 2020 and 2021, Susan et al. reported [78,79] novel magnetic activated charcoal-β-cyclodextrin-alginate polymer nanocomposite MNP@AC@CD@Alg to adsorb cationic dyes, drugs, and metals from aqueous solutions via physico-chemical adsorption mechanism (Table 7, Entry 6). In the presence of calcium, sodium alginate forms a complex due to the presence of carboxylic and hydroxyl functions. The combination of sodium alginate-based material and cyclodextrin support enhances the

remediation absorption capacities of the composite gel beads. The synthesized material is a mesoporous material with particle sizes around 20 nm, with rough pores around 2–16 nm, available to encapsulate dyes. The irregular structure and large surface area obtained enhance the beads' adsorption properties. The crystalline phases were observed by XRD with the face-centered cubic (fcc) structure of Fe_3O_4 with crystallite sizes of MNP@AC, MNP@AC@CD, and MNP@AC@CD@Alg of 11.04, 2.71, and 5.63 nm, respectively. The presence of alginate and CD has been confirmed by FTIR analysis, especially with the band at 1408 cm^{-1} attributed to the symmetric stretching vibration peak of carboxylate function. The thermal analysis showed that the addition of a carbon material and iron nanoparticles increased the thermal stability of polymer gel beads. Three phases of weight loss occurred with the residual water from 39–133 °C (5.53%), from 234–314 °C (19.8%) due to the immobilized polymer matrix (CD and alginate), and 41.38% weight loss from 415–503 °C due to the decomposition of oxygen-containing groups and carbon framework. Magnetic-hysteresis (MH) loops of the final composite MNP@AC@CD@Alg were observed by VSM, confirming the ferrimagnetic properties of the nanoparticles with very low saturation magnetization of 0.128 emu/g due to the alginate coating. These results indicate that the Fe_3O_4, AC, CD and SA were successfully combined to form the polymer gel beads. A magnetic cyclodextrin polymer using epichlorohydrin crosslinker from Fe_3O_4 nanoparticles was published by Gabaldon et al. [80] (Table 7, Entry 7). In these reaction conditions, the coating of metallic particles by β-CD-EPI polymer was maintained by hydrogen bond interactions and coordination chelation between the hydroxyl groups and the oxygen atoms present on the polymer and the iron metal at the magnetite surface. No defined shape images were observed, suggesting heterogeneous surface morphology and an irregular structure of the polymer. The beads showed a glass transition around 189 °C before any decomposition took place. This transition phenomenon, attributed to relaxation of the structure to a more flexible arrangement, was absent in the EPI-β-CD polymer or in any of the starting materials. The authors studied the adsorption of direct red 83:1. This dye mainly exists as anionic forms in the range of pH = 3–7 corresponding to four sulfonate groups. The negative charges present both in the dye and the adsorbent cause repulsive forces decreasing the adsorption capacity. In 2023, Han et al. [81] developed single and co-adsorption of methylene blue by magnetic β-cyclodextrin based on alginate and biochar (AC) as biosupports using microwave activation (Table 7, Entry 8). Pyrolysis of biodegradable rice straw (300 °C for 2 h) in an oxygen-free environment led to relatively low-cost biochar. To enhance the pollutant removal performance, alginate was used to introduce acid and hydroxyl functional group on the material surface. As grafting β-CD onto biochar with a crosslinking agent can be time-consuming, microwave irradiation was applied, generating vibration and friction between molecules and a fast increase of the medium temperature (hot-spot effect), accelerating the kinetics of the reaction (hours to seconds). The protocol reported is very simple and consists of mixing all the ingredients Fe_3O_4, β-CD, and biochar in the presence of NaH_2PO_4, EDTA, and Macrogol 1000 in a microwave at 136 W at 40 °C for 1 h. No problems due to the magnetic properties of the iron nanoparticles and the instability of the cyclodextrin under these conditions were underlined by the authors. Then AC@MNP@CD obtained was mixed with sodium alginate, and $CaCl_2$ solutions were introduced using a dropper, leading to a ligand-metal complex. Through SEM images, the pores of biochar could still be detected, and spherical nanoparticles were observed on the surface. FT-IR spectra showed the aromatic molecules issued from biochar generating C=C vibration around 1559 cm^{-1}, and the peaks at 1417 and 1620 cm^{-1} were associated with the vibration stretching of symmetrical and unsymmetrical O–C–O of sodium alginate. XRD patterns exhibited peaks of at $2\theta = 20.81°$ (Biochar), 22.25° (β-CD), 30.09°, 35.42°, 43.05°, 56.94°, and 62.51° (Fe_3O_4). The magnetization value for β-CD@MBCP was identified as 6.77 emu/g due to the alginate coating.

Table 7. A summary of MNP-CDs prepared via a noncovalent binding strategy.

Entry	Synthetic Scheme	Dye/Use	Ref.
1	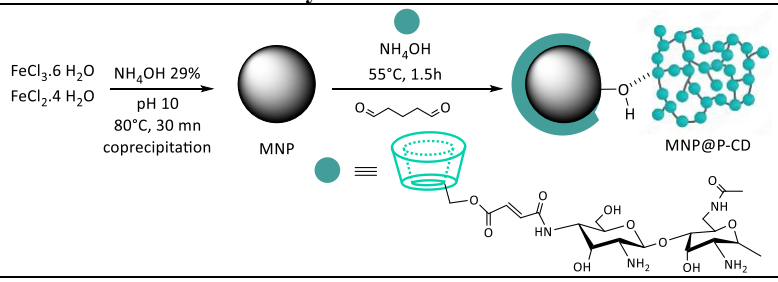	Methyl blue Desorption 0.1 M in ethanol	[73]
2	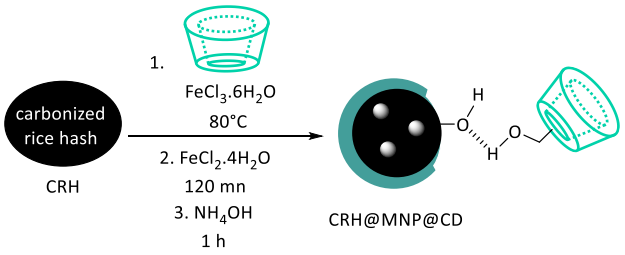	Methylene blue Desorption in ethanol	[74]
3	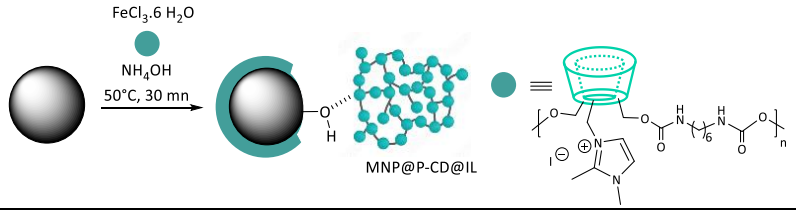	Rhodamine B Desorption SDS, CTAB, methanol, ethanol, 0.1 M NaOH, 0.1 M HCl	[75]
4	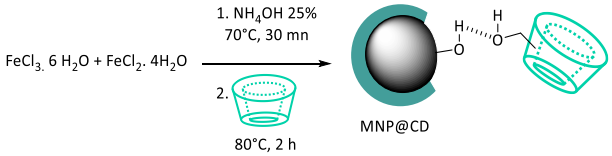	Eosine Phloxine	[76]
5	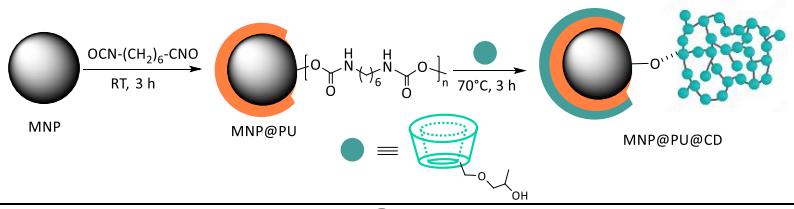	Methyl volet	[77]
6	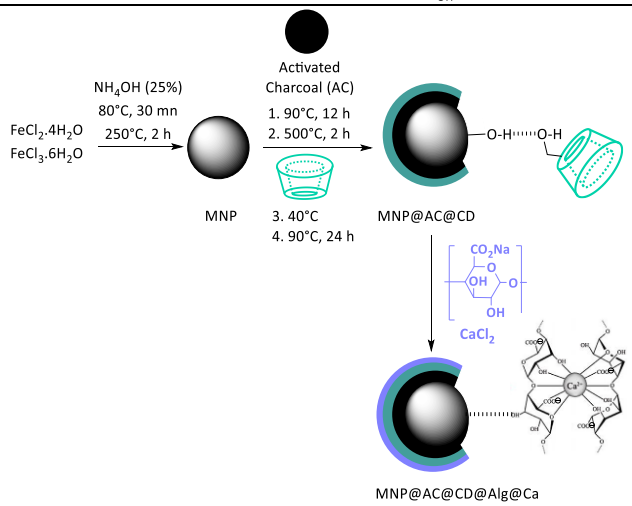	Methyl violet Brilliant green Norfloxacin Ciprofloxacin Cu(II) Desorption 0.1 M HCl for dyes 0.005 M NaCl for drugs and 0.01 M EDTA for metal ions	[78,79]

7	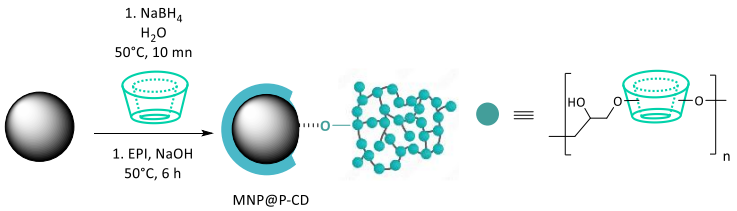	Direct red 83:1 Desorption Acetate buffer pH 4, 30 min	[80]
8	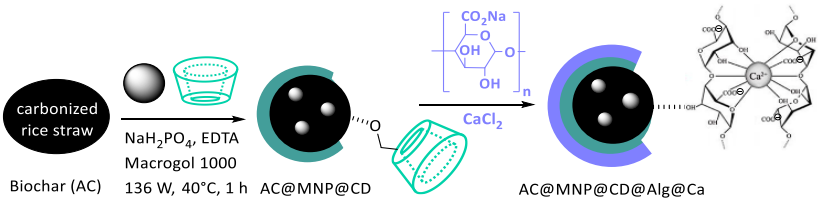	Methylene blue Desorption 0.1 M HCl, methanol	[81]

3. Results: Binding of Dye Molecules by CDs and MNP@CD

There have been numerous studies on the inclusion complexes of various guest dyes by cyclodextrin host molecules in aqueous solution; these have recently been surveyed in a book chapter [82]. For example, Moritz and Sahyun reported spectroscopic studies of the binding of cyanine dyes by β-CD over 20 years ago [83]. More recently, Saifi et al. reported the binding of an azo dye by β-CD [84], and discussed the potential of this complexation for water purification [84]. However, neither of these papers reported values of the binding constant K, which is critical for the applications of CDs themselves and CD-based adsorbent materials in the remediation of dye pollutants from natural water. In the following, representative studies that report the values of K will be reviewed and discussed. These include a wide range of dye guest molecules as well as different native and modified cyclodextrins. The reported values of K from these publications are summarized in Table 8. It is difficult to establish a correlation between the CD grafting content on MNP and the amount of adsorbed dye due to the absence of quantification titration of free accessible cavities. The grafting rate extracted from TGA experiments is not accurate enough for such a comparative analysis. Moreover, quantification of the synergic effects of various molecular interactions is difficult to measure.

In an early paper, the inclusion of resorcinol-based acridinedione dyes in β-CD at various temperatures was studied via fluorescence enhancement studies [85], and in the case of the *N*-phenyl substituted dye, a relatively low binding constant of 401 M^{-1} at 298 K was obtained. This study also reported the thermodynamics of this binding, and found that both the enthalpy and entropy of binding were negative, indicating that inclusion of this dye into β-CD is enthalpy driven. They attributed the large negative enthalpy to the presence of the hydrophobic effect as the main driving force for inclusion, and the decrease in entropy to the loss of rotational motion of both the host and guest upon complexation. In an extensive study, Liu et al. reported the binding constants for six different dye molecules in all three native CDs, as well as several mono-substituted modified CDs using fluorescence titrations [86]. Acridine red was studied in all of the CDs, and the values of the binding constants are listed in Table 8. As can be seen from the table, in comparing the three native CDs, the largest K of 1380 M^{-1} was obtained with β-CD, with much smaller values in both α-CD (49.7 M^{-1}) and γ-CD (117 M^{-1}). Thus, the size of the β-CD cavity is the best match for the size and shape of this particular dye; this is a commonly observed result for dye molecules. In the case of Acridine red in the modified mono-substituted β-CDs, the binding constants were either similar to, or in most cases significantly larger than, that for β-CD itself. For example, in the case of BzSe-β-CD, in which one of the primary hydroxyls on the smaller rim was substituted by $CH_2SeCH_2C_6H_6$, a large value of K of 8050 M^{-1} was obtained, indicating the role of the substituent group in facilitating the binding of the dye. Other dyes were also reported with β-CD, with crystal violet showing a stronger binding than acridine red, with K = 5850 M^{-1}, whereas fluorescein showed a much weaker binding, with K = 11.7 M^{-1}.

Table 8. Representative reported binding constants K for the inclusion of dyes in various cyclodextrins at 298 K.

Cyclodextrin	Dye *	K (M^{-1})	Reference
β-CD	Acridine red	49.7	[86]
	Methyl orange	2527	[87]
β-CD	N-phenylacridinedione	401	[85]
	Acridine red	1380	[86]
	Crystal violet	5850	[86]
	Fluorescein	11.7	[86]
	Direct red 83:1	7590	[88]
	Methyl orange	952	[87]
	Methylene blue	310	[89]
BzSe-β-CD	Acridine red	8050	[86]
DM-β-CD	Direct yellow 106	2.26×10^6	[88]
TM-β-CD	Direct yellow 106	5.00×10^6	[88]
	Direct red 83:1	1.98×10^4	[88]
HP-β-CD	Direct red 83:1	1.08×10^4	[88]
β-CD	Acridine red	117	[86]
	Direct yellow 106	1.03×10^5	[88]

* The structure of Methylene Blue is shown in Figure 1b; the structure of all other dyes reported in the table can be found in the original references.

These values illustrate the crucial importance of the size and shape match between the dye guest and the cyclodextrin cavity, and that binding constants need to be measured for any specific CD-dye pair of interest. Scott et al. reported the binding of methylene blue using UV-vis absorptance studies [89]. This dye is of particular interest, as it is important both industrially and in medical and other applications, and is often used as a representative dye in water remediation studies. They reported a moderate binding constant of 310 M^{-1} in β-CD. They found that the binding of methylene blue by β-CD resulted in a reduction of its cell staining and glucose uptake effects. Semeraro et al. published an extensive study on the binding of two large, related dyes, direct Red 83:1 (DR) and direct yellow 106 (DY), using both spectrophotometric and electrochemical techniques [88]. In the case of DR, they obtained a value of K of 7590 M^{-1} in β-CD, but larger values of 1.98×10^4 and 1.08×10^4 M^{-1} in trimethyl-β-CD (TM-β-CD) and 2-hydroxypropyl-β-CD (HP-β-CD). In the case of the larger DY, they obtained a very large value of K of 1.03×10^5 M^{-1} in γ-CD, and even larger values of 2.26×10^6 and 5.00×10^6 M^{-1} in dimethyl-β-CD (DM-β-CD) and TM-β-CD. In the case of the larger DY and the native CDs, the larger γ-CD cavity gave a stronger binding, again illustrating the importance of the size match between host and guest. However, the two modified β-CDs gave even stronger binding, dramatically illustrating the superior binding properties of modified CDs. As a final illustrative example, Barão et al. compared the binding of methyl orange in α- and β-CD at pH 3.0 in a disodium citrate-phosphate buffer, which proved to be the best conditions for the inclusion complexation [87]. They reported K values of 2527 and 952 M^{-1} for α- and β-CD, respectively, showing that in this case, the smaller CD cavity gave better binding; this is consistent with the relatively small size of methyl orange, a diazo dye with benzene rings only, again illustrating the importance of the match between the guest and host cavity sizes.

Studies have also been reported on the binding of dyes by cyclodextrin polymers [13,63], nanosponges [90], and other CD-based adsorbents [14]. The applications of such CD-based materials to the removal of water pollutants have also been proposed and reviewed [6,7,14], including a 2021 review of magnetite nanoparticles in general as dye sorbents [91]. However, for the purpose of this review, the focus will be on CD-decorated magnetic nanoparticles (MNP@CD) for water remediation, and their ability to trap dye pollutants. In aqueous solution, an equilibrium is established between the free and bound dye molecules, which is typically well described by the Langmuir isotherm model. This model, and its application to

magnetic nanoparticles as adsorbents, is well described in detail in reference [91], along with tables of reported Langmuir isotherm parameters for a wide range of magnetic nanoparticles. In the case of MNP@CD, a number of different interactions can occur between the magnetic nanoparticles, the appended cyclodextrin cavities, and the dye molecules, as illustrated in Figure 8.

A convenient measure of the dye adsorbing abilities of MNP@CD is the adsorption capacity, defined as the mass of dye molecules adsorbed per unit mass of MNP@CD, with units typically of mg/g. Table 9 summarizes the reported dye adsorption capacity of a number of MNP@CD, with a range of specific dyes; these studies will be described in the following.

The first study to report the removal of a dye by a cyclodextrin-derivatized magnetic nanoparticle was that of Badruddoza et al. in 2010 [57]. They prepared a carboxymethyl-β-cyclodextrin conjugated magnetic nanoparticle using two different synthetic methods: via covalent bonding (MNP(C)@CMCD) and by co-precipitation (MNP(CP)@CMCD). They used the well-studied dye methylene blue (Figure 1b) as a representative dye, and found that their magnetic nano-adsorbents could significantly adsorb this dye, with adsorption capacities of 140.8 and 277.8 mg/g for the covalently and co-precipitation prepared materials, respectively. Other groups also used methylene blue as the target dye for their MNP@CD. Lv et al. synthesized a bioadsorbent (RH-c/Fe_3O_4/CD), which had an adsorption capacity for methylene blue of 359.8 mg/g, higher than that of Badruddoza et al. Liu et al. prepared magnetic nanospheres functionalized by β-CD polymers (P-CD), which had a similar adsorption capacity of 305.8 mg/g [60]. An even higher adsorption capacity was reported by Xie et al., whose Fe_3O_4/CD-polymer composite (CDP-Fes) showed a high affinity for methylene blue, with an adsorption capacity of 565 mg/g [65]. Yadav et al. prepared a novel magnetic CD nanocomposite incorporating activated charcoal (Fe_3O_4/AC/CD/Alg), which had a modest adsorption capacity for methylene blue of 10.63 mg/g in its dry powder form [78]. Most recently, Sabzevar et al. reported a large adsorption capacity for methylene blue of 454.54 mg/g using a CD/magnetic lignin adsorbent (β-CD-TA-MKL) [70]. Other dyes have also been the subject of MNP@CD adsorption studies. Fan et al. prepared cyclodextrin-chitosan magnetic nanoparticles (CDC), and found a very large adsorption capacity of 2780 mg/g with methyl blue through host-guest interactions [73]. Cai et al. prepared ammonium β-CD-conjugated magnetic nanoparticles (GEPCD-MNP), and found a strong adsorption capacity of 389.1 for Congo red [64]. Another carboxymethyl-β-CD-based adsorbent (Fe_3O_4/CM-CD) was synthesized by Hu et al.; it showed a moderate adsorption capacity of 203.54 mg/g for C.I. basic blue [62]. Nasiri et al. synthesized a hydroxypropyl-β-CD-polyurethane magnetic conjugate (HPMNPU), and tested it with two different dyes [77]. They found extremely high adsorption capacities of 1269 and 1667 mg/g with crystal violet and methyl violet, respectively, indicating a very high dye capacity for this particular MNP@CD. As a last example, Liu et al. extended their study of the adsorption of methylene blue by their CD nanocomposite incorporating activated charcoal (referred to as Fe_3O_4/AC/CD/SA) to methyl violet and brilliant green, again with relatively low adsorption capacities of 5.552 and 2.283 mg/g, respectively [79]. Interestingly, this value for methyl violet is nearly three orders of magnitude lower than that reported by Nasiri et al. for their HPMNPU material.

It is clear from these reports that MNP-CDs with a wide range of adsorption capacities for methylene blue and other dyes have been prepared for potential applications in the remediation of dye-polluted wastewater. In general, the greater the adsorption capacity, the more useful MNP@CD will be for such applications. Some of these materials discussed in this section, as well as other MNP@CDs, have been directly applied to the removal of dyes from wastewater samples. The success of such remediation methods will be discussed in Section 4, for methylene blue as well as other dyes.

Table 9. Representative reported dye adsorption capacities of MNP@CDs at 298 K.

Dye *	MNP-CD **	Adsorption Capacity (mg/g)	Reference
Methylene blue	CMCD@MNP(C)	140.8	[57]
	CMCD@MNP(P)	277.8	[57]
	RH-c/Fe_3O_4/CD	359.8	[74]
	P-MCD	305.8	[60]
	CDP-Fes	565	[65]
	Fe_3O_4/AC/CD/Alg	10.6	[78]
	β-CD-TA-MKL	454.5	[70]
Methyl blue	CDCM	2780	[73]
Congo red	GEPCD@MNP	389.1	[64]
C.I. basic blue	Fe_3O_4/CM-CD	203.5	[62]
Crystal violet	HPMNPU	1269	[77]
Methyl violet	HPMNPU	1667	[77]
	Fe_3O_4/AC/CD/SA	5.9	[79]
Brilliant green	Fe_3O_4/AC/CD/SA	2.3	[79]

* The structure of Methylene Blue is shown in Figure 1b; the structure of all other dyes reported in the table can be found in the original references. ** The MNP-CD abbreviations listed are those used in the original references; the detailed compositions can be found there as well.

4. Results: Remediation Applications of MNP@CDs

The adsorption capacity of a number of MNP@CDs for various dyes was discussed above. However, to test their usefulness in remediating wastewater, studies need to be performed on actual or simulated dye-contaminated waters, to test the efficiency (as % dye removal from the wastewater sample), the recyclability/reusability of the adsorbent materials, and the water volume capacity. In each case, the method for removing the dyes from the MNP@CD after adsorption from the water sample needs to be optimized; this typically involves using an organic solvent such as methanol. Such studies will be discussed in this section, some of which were reviewed above for their dye adsorption efficiencies. Table 10 summarizes the reported % dye removal and recyclability for a range of dye and MNP@CD combinations. Part of this application involves the optimization of the method.

A number of studies have focused on the removal of methylene blue from aqueous dye solutions, and a number of those were discussed above in Section 3 in terms of their adsorption capacities. Liu et al. applied their CD-polymer-functionalized magnetic nanospheres P-MNS to the removal of methylene blue from simulated wastewater samples [60]. They found a very high removal efficiency of 99.98%, and a good recyclability, with 86% absorption efficiency achieved after five trials. Similarly, Xie et al. with their CDP-Fes material found a maximum removal rate of 99.27%, and an adsorption capacity of 93% of its initial value after 4 cycles [65], and Yadav et al. with their Fe_3O_4/AC/CD/Alg material reported a maximum removal rate of 97.7%, and an adsorption capacity of 92% of its initial value after 4 cycles [78]. Most recently, Sabzevar et al. reported that their β-CD-TA-MKL magnetic lignin material showed a maximum removal efficiency of 96.24%, which only declined to 91.10% after five cycles, which is 95% of the initial value, proving an excellent recyclability for this adsorbent material. Chen et al. did an interesting study of the simultaneous removal of methylene blue and Pb(II) using a β-CD modified magnetic alginate/biochar material (β-CD@MBC_p) [81]. They found a high degree of renewability in the combined uptake after four stepwise cycles. The authors proved that methylene blue was retained by inclusion into the cavity via host-guest interactions, π-π stacking between the C=C bond of the dye and the biochar and, hydrogen bonding formation through the dye and the -OH and -COOH groups on the surface of the β-CD@MBC_p.

Whereas the studies on methylene blue reported in the paragraph above were performed using prepared aqueous solutions of methylene blue, Hu et al. used actual dying wastewater samples [66]. They used a

green synthesis approach to prepare a material which they referred to as MNP-CM-CDP, and tested its ability to remove a range of model pollutants, including methylene blue, from spiked sewage plant wastewater. They found 93.5% removal of methylene blue from wastewater samples from a sewage plant spiked with the dye, and high recyclability, with the adsorption efficiency decreasing by only 5.79% after five cycles.

Table 10. Representative reported MNP@CD dye removal efficiencies and recyclability from wastewater samples.

Dye *	MNP-CD **	Max % Removal	Recyclability ***	Reference
Methylene blue	P-MCD	99.98	86% after 5 trials	[60]
	CDP-Fes	99.28	93% after 4 trials	[65]
	Fe_3O_4/AC/CD/Alg	97.7	92% after 4 trials	[78]
	β-CD-TA-MKL	96.24	92% after 4 trials	[70]
	MNP-CM-CDP	93.5	94% after 5 trials	[66]
Malachite green	SPNA	-	Consistent over 5 trials	[56]
	MNP-CD	96.5–100.5	-	[55]
Methyl blue	CDCM	-	Consistent over 4 trials	[73]
	QMCDP1	96.84	79% after 5 trials	[69]
Eosin	CD@MNP	62	-	[76]
Congo red	GEPCD@MNP	-	90% after 5 trials	[64]
Methyl orange	Fe_3O_4-PEI/β-CD	-	Consistent over 5 trials	[59]
C.I. basic blue	Fe_3O_4/CM-CD	74	94% after 6 trials	[62]
Crystal violet	MNP@CD	96.5–100.5	-	[55]
Methyl violet	HPMNPU	96.1	-	[77]
Basic fuschin	Fe_3O_4@CD	95.6	79% after 5 trials	[67]

* The structure of Methylene Blue is shown in Figure 1b; the structure of all other dyes reported in the table can be found in the original references. ** The MNP-CD abbreviations listed are those used in the original references; the detailed compositions can be found there as well. *** Expressed as the % of initial adsorption capacity or % removal rate after the stated number of trials, or as the number of trials with consistent results before a significant decrease was observed.

Another often-studied dye in this area of research is malachite green, a synthetic blue-green dye used in industrial textiles and also as a fish aquarium antifungal. Yadav et al. prepared a maleic anhydride/β-CD-based superparamagnetic nanoabsorbent (SPNA) and observed consistent adsorption/desorption results over five cycles, but a drop-off thereafter [56]. Methylene blue, malachite green and rhodamine 6G connect with the magnetic support by electrostatic and Van der Waals interactions. Additional hydrogen bonding and host-guest interactions occurs only for the methylene blue and malachite green; rhodamine 6G being too hydrophobic and with larger size. Shahrebabak et al. prepared a silica-coated poly(β-CD-ester)-functionalized MNP@CD, and most importantly applied it to the removal of malachite green (as well as crystal violet) to real natural water samples, including tap water, fishpond water, and lake water [55]. They reported high, near-quantitative recoveries in the range of 96.5% to 100.5% for malachite green, and similar values for crystal violet, as can be seen in Table 10. The authors did not report the recyclability of this material.

Other dyes have also been studied as target pollutants for removal from water samples. These include methyl blue [69,73], various azo dyes [51], Rhodamine B [75], eosin [68,76], Congo red [64], methyl orange [59], C.I. basic blue [62], crystal violet [55,77], methyl violet [77], and basic fuschin [67]. Where reported, the removal efficiency and/or recyclability parameters from these studies are also listed in Table 10.

A different approach to water remediation using MNP@CDs involves their use in concentrating and facilitating photocatalytic degradation of dye molecules, instead of their direct removal [91–95]. Rodruguez-Lopez et al. used magnetic CD polymers with pulsed light to destroy azo dyes in wastewater [80]. Yadav et al. utilized an MNP@CD material as a photocatalyst for the removal of malachite green from wastewater samples, achieving 89.4% removal in 120 min, through host-guest inclusion [92]. Most recently, Kaur et al. used a magnetic CD/Fe_2O_3 nanocomposite fabricated with β-CD to treat wastewater

by photolytically degrading a range of industrial dyes, including methylene blue [92]. The methylene blue and methyl orange remediation process takes place due to multilayer adsorption on the nanocomposite surface via H-bonding interactions between the nitrogen atom of the dyes and -OH group of the β-CD, electrostatic interactions between ammonium from methylene blue and sodium sulfonate from methyl orange, and -OH groups of the oligosaccharidic crown, and finally, via van Der Waals forces. In addition, Lighcan et al. used an *N*-heterocyclic Cu(II) complex appended to an MNP@CD to provide redox catalytic reduction of a wide range of industrial dyes [68]. They found a high catalytical activity, which, combined with magnetic recovery of the catalyst, indicated a high potential for the catalytic reduction of industrial dyes in real wastewater applications.

5. Comparison of Different MNP@CD and Recycling

As discussed above, there has been a diverse range of CD-appended magnetic nanoparticles synthesized in recent years, with varying success and utility towards the removal of industrial dye pollutants from natural and simulated wastewater samples, so it is important to compare the success and utility of these different MNP@CDs. One of the most important experimental measures of the potential use for this purpose is the dye adsorption capacity, the mass of dye able to be absorbed per g of MNP@CD. These values from the literature, which were reported, are summarized in Table 9 for a variety of industrial dyes. As can be seen from the table, there is a large range in reported adsorption capacities, from a low of 2.283 mg/g for the dye brilliant green in an MNP@CD based on activated charcoal particles [79] to a very large value of 2780 mg/g for methyl blue in a chitosan-based MNP@CD at 30 °C [73]. This is a three orders of magnitude range in adsorption capacity! Interestingly, this highest adsorption capacity of 2.78 g/g was reported from one of the first reports of an MNP@CD applied to the removal of an industrial dye, back in 2012; this value has not been surpassed since (although two other studies were also above 1 g/mg). It is clear that these values are highly dependent on both the dye itself in terms of its size and shape, and the properties of the MNP@CD, making comparisons between studies and correlations between MNP structures and binding capacity difficult to establish. In addition, experimental conditions, including dye concentration, solution pH, and temperature have all been shown to impact these values, and in each case, optimization of conditions was necessary to maximize the adsorption capacity value. All of these factors have undoubtedly contributed to the wide range of binding capacities reported. To compare the capacities of different MNP@CDs, it is useful to compare the values for the same dye molecule, to allow for a valid comparison. For this purpose, methylene blue is the best dye to choose, as it has been studied in the most MNP@CD materials, a total of seven listed in Table 9. The MNP@CD with the highest ability to absorb methylene blue is the β-CD-TA-MKL material synthesized and studied by Sabvezar et al., with an impressive adsorption capacity of 455 mg/g.

When considering the maximum percentage removal of the dyes from aqueous samples, as listed in Table 10, there was a range of values from 62 to close to 100%, with the majority of the MNP@CDs giving values above 95%. Thus, from this perspective, most of the MNP@CDs performed equally well, with just two with values less than 90%. Once the method for both adsorption and removal of the dye was obtained, in terms of recyclability, which is also listed in Table 10, most of the MNP@CDs studied had similar results, with most maintaining their adsorption capabilities for four to five cycles. The best reported recyclability was that of Fe_3O_4/CM-CD, which retained 94% of its initial adsorption ability after six adsorption and removal cycles [62].

Overall, most of the MNP@CDs reported had strong adsorption capacities, which allowed for good dye removal and recyclability, so the choice of an MNP@CD for a particular remediation application would depend on the specific dye or dyes involved, as well as the ease, cost, and environmental impact of the specific synthetic procedures.

It is also useful to summarize the comparison of the synthetic procedures and formation conditions involved for different MNP@CDs; these are summarized in Table 11 (coprecipitation method) and Table 12 (autoclave activation).

Table 11. Formation conditions of MNPs particles by the co-precipitation method from the literature. * iron, reagents, and β-CD are mixed together to form MNPs. Otherwise, MNPs are first produced in a first step, and immobilization of β-CD is done in a second step.

Co-Precipitation Fe^{2+}, Fe^{3+}			
Reagents	**Temperature**	**Time**	**Ref.**
NH_3, β-CD	50 °C	30 min	[52]
	80 °C	30 min	[53,54,57,64,73,78–80]
	80 °C	5 h	[63]
NH_3, β-CD *	80 °C	30 min	[76]
NH_3, SDS in xylene, β-CD	80 °C	3 h	[51]
NH_3, sodium citrate, β-CD	-	30 min 1 h	[67]
NH_3, carboxymethylated-β-CD *	80 °C	2 h	[62]
NH_3, lignin, β-CD	80 °C	1 h	[70,71]
NH_3, carbonated rice husk, β-CD *	80 °C	-	[74]
NH_3, ionic liquid, β-CD polymer *	55 °C	30 min	[75]
NaOH, Tetrafluoroterephtalonitrile cross-linked β-CD *	90 °C	24 h	[65]
NH_3, polymer from carboxymethylated β-CD, epichlorhydrin *	90 °C	1 h	[66]
NaOH, polymer from carboxymethylated β-CD, epichlorhydrin *	Microwave 2.45 GHz	30 min	[68]
NaH_2PO_4, Biochar, EDTA, Macrogol 100, β-CD	Microwave 40 °C	1 h	[81]

Table 12. Formation conditions of MNPs particles by autoclave activation from the literature. * iron, reagents, and β-CD are mixed together to form MNPs. Otherwise, MNPs are first produced in a first step, and immobilization of β-CD is done in a second step.

Autoclave			
Reagents	**Temperature**	**Time**	**Ref.**
Fe^{3+}, Sodium acetate, PEG-6000, Ethylene glycol	200 °C	8 h	[77]
Fe^{3+}, Trisodium citrate, Sodium acetate, PEG-6000	200 °C	8 h	[58]
Fe^{3+}, Sodium acetate, Ethylene glycol, 1,6-hexadiamine	200 °C	8 h	[59]
Fe^{3+}, Sodium acetate, Ethylene glycol, β-CD *	200 °C	8 h	[60]
Fe^{3+}, Sodium acetate, PEG 600	200 °C	16 h	[55]
Fe^{3+}, Trisodium citrate, Sodium acetate, Ethylene glycol	200 °C	10 h	[69]
Fe^{2+}, Fe^{3+}, NH_3, β-CD Hexamethylene bis(hexadecyldimethylammonium bromide) (16–6–16) * or Tris(2-*N*(dodecyl *N,N*-dimethylammonio)ethylamine) tribromide (TriCAT) *	150 °C	24 h	[61]

6. Conclusions

A wide variety of MNP@CD have been prepared and utilized over the past quarter century for the remediation of dye-contaminated wastewater samples. All of these magnetic materials have a significant advantage over other types of sorbent materials, namely their ease of removal from the water sample being treated, using a simple magnet. Two main strategies based on covalent or noncovalent bonding can be applied to immobilize β-cyclodextrins or polymers of cyclodextrins on iron nanoparticles. The covalent links use silica coating, autoclave, plasma, microwave activations or binding with carboxylation reaction, generating functionalized nanoparticles that are physically and chemically more resistant. However, co-precipitation reactions are widely used and involve hydrogen bonding interactions between the entities. Composites are also synthetized using biomass such as activated carbon, biochar, chitosan, alginate to

reduce the environmental impact of the synthesis. Other additives, such as ionic liquids, can also bring a synergic effect on the pollutant capture capacity of the magnetic material. The resulting MNP@CD have a wide range of abilities to adsorb industrial dyes, with reported values of the adsorption capacities spanning a range of 3 orders of magnitude, from 2.38 to 2780 mg of dye per g of MNP@CD. This value depends strongly on the characteristics of both the dye and the MNP@CD, as well as other factors such as dye concentration, pH, and temperature. Many of these materials were also tested for their ability to remove specific dyes from simulated or (less frequently) real dye-contaminated wastewater samples. Again, a range of efficiencies was reported, in terms of the percent removal of the contamination dye, but in the majority of cases excellent removal rates of 90% or above have been obtained. Recyclability of the MNP@CD is also of primary importance, and in the majority of cases, good adsorption abilities were found after five repeated adsorption/removal cycles, with a highest recyclability reported of a retention of 96% of the adsorption capacity after six cycles. These results show that there is significant promise for the application of MNP@CDs to the remediation of industrial dye-contaminated natural waters.

In all cases, the magnetization properties decrease with the increase of coating on the iron core. However, the MNP@CD can still be extracted using a simple magnet. Surprisingly, the strength of the magnet and the conditions of magnetization are never discussed or optimized. Indeed, for an industrialization application, this technical point would have to be studied. In fact, we noted very few tests on real wastewater and no industrial scale up using magnetic pollutant extraction. In this perspective, the recyclability of the MNP is still low (4–5 cycles), and the authors do not explain if the MNP@CD are clogged or if the alcohol washing treatment is not efficient enough to carry on the extraction process. In addition, only a few studies report an association constant between dye and MNP@CD, and the number of accessible cavities of CD is never estimated. The lack of grafting rate and titration measurement of CD cavities available do not allow for a comparison of the strategies nor for any correlations to be established between remediation capacity and physical properties of the MNP@CD.

Lastly, other upcoming MNP@CDs could also extract and degrade by photocatalysis the pollutant at the same time; the dyes themselves are usually not stable and hence cannot be recycled after extraction. Future work includes more efficient, greener synthetic approaches, testing on real natural water samples, and upscaling of the laboratory-based procedures for direct application to the remediation of actual large-scale contaminated natural waters.

Acknowledgments

This work was partially supported by Normandie University, the Region Normandie, the Centre National de la Recherche Scientifique, University Rouen Normandie, INSA Rouen Normandie, University Caen Normandie, ENSICAEN, Labex SynOrg (ANR-11-LABX-0029), the graduate school for research XL-Chem (ANR-18-EURE-0020 XL CHEM), Innovation Chimie Carnot (I2C), and the University of Prince Edward Island, Charlottetown, PE C1A 4P3, Canada.

Author Contributions

Conceptualization, G.G. and B.D.W.; Methodology, G.G., C.B. and B.D.W.; Writing—Original Draft Preparation, G.G. and B.D.W.; Writing—Review & Editing, G.G., C.B. and B.D.W.; Visualization, G.G., C.B. and B.D.W.; Supervision, G.G.

Ethics Statement

Not applicable.

Informed Consent Statement

Not applicable.

Data Availability Statement

This is a review article only, with no new data. All data availability would be obtained through the referenced articles.

Funding

This research received no external funding.

Declaration of Competing Interest

The authors declare that they have no known competing financial interests or personal relationships that could have appeared to influence the work reported in this paper.

References

1. Islam T, Repon M, Islam T, Sarwar Z, Rahman MM. Impact of textile dyes on health and ecosystem: A review of structure, causes, and potential solutions. *Environ. Sci. Poll. Res.* **2023**, *30*, 9207–9242. DOI:10.1007/s11356-022-24398-3
2. Chung KT. Azo dyes and human health: A review. *J. Environ. Sci. Health C Environ. Carchinog. Ecotoxicol. Rev.* **2016**, *34*, 233–261. DOI:10.1080/10590501.2016.1236602
3. Moradi O, Sharma G. Emerging novel polymeric adsorbents for removing dyes from wastewater: A comprehensive review and comparison with other adsorbents. *Environ. Res.* **2021**, *201*, 111534. DOI:10.1016/j.envres.2021.111534
4. Shi Y, Chang Q, Zhang T, Song G, Sun Y, Ding G. A review on selective dye adsorption by different mechanisms. *J. Environ. Chem. Eng.* **2022**, *10*, 108639. DOI:10.1016/j.jece.2022.108639
5. Elgoyhen J, Tomovska R. Advanced Technologies for Wastewater Treatment: Graphene-Based Catalysts. *Molecules* **2025**, *30*, 3405. DOI:10.3390/molecules30163405
6. Kumari P, Singh P, Singhal A, Alka. Cyclodextrin-based nanostructured materials for sustainable water remediation applications. *Environ. Sci. Pollut. Res.* **2020**, *27*, 32432–32448. DOI:10.1007/s11356-020-09519-0
7. Liu Q, Zhou Y, Lu J, Zhou Y. Novel cyclodextrin-based adsorbents for removing pollutants from wastewater: A critical review. *Chemosphere* **2020**, *241*, 125043. DOI:10.1016/j.chemosphere.2019.125043
8. Li Y, Liu F, Abdiryim T, Liu X. Cyclodextrin-derived materials: From design to promising applications in water treatment. *Coord. Chem. Rev.* **2024**, *502*, 215613. DOI:10.1016/j.ccr.2023.215613
9. Liu C, Crini G, Wilson LD, Balasubramanian P, Li F. Removal of contaminants present in water and wastewater by cyclodextrin-based adsorbents: A bibliometric review from 1993 to 2022. *Environ. Pollut.* **2024**, *348*, 123815. DOI:10.1016/j.envpol.2024.123815
10. Urooj T, Mishra M, Pandey S. Unlocking environmental solution: A review of cyclodextrins in pollutant removal. *Discover Environ.* **2024**, *2*, 65. DOI:10.1007/s44274-024-00090-w
11. Fouda-Mbanga BG, Tywabi-Ngeva Z, Badawy WM, Ebite C, Onotu OP, Adogidi C, et al. Green cyclodextrins-derivatives for sustainable remediation of pesticides and heavy metals: A review. *J. Molec. Struct.* **2025**, *1328*, 141326. DOI:10.1016/j.molstruc.2025.141326
12. Lacalamita D, Mongiovi C, Crini G, Morin-Crini N. Cyclodextrins for the removal of per- and polyfluoroalkyl substances: A review. *Environ. Chem. Lett.* **2025**, *25*, 1713–1743. DOI:10.1007/s10311-025-01868-x
13. Crini G. Studies on adsorption of dyes on beta-cyclodextrin polymer. *Biores. Technol.* **2003**, *90*, 193–198. DOI:10.1016/S0960-8524(03)00111-1
14. Amran F, Zaini MAA. Beta-cyclodextrin adsorbents to remove water pollutants—A commentary. *Front. Chem. Sci. Eng.* **2022**, *16*, 1407–1423. DOI:10.1007/s11705-022-2146-2
15. Safapour S, Mazhar M, Nikanfard M, Liaghat F. Recent advancements on the functionalized cyclodextrin-based absorbents for dye removal from aqueous solution. *Int. J. Environ. Sci. Technol.* **2022**, *19*, 5753–5790. DOI:10.1007/s13762-021-03671-x
16. Kakhki RM. Application of magnetic nanoparticles modified with cyclodextrins as efficient adsorbents in separation systems. *J. Incl. Phenom. Macrocycl. Chem.* **2015**, *82*, 301–310. DOI:10.1007/s10847-015-0512-0

17. Mishra S, Yadav MD. Magnetic Nanoparticles: A Comprehensive Review from Synthesis to Biomedical Frontiers. *Langmuir* **2024**, *40*, 17239–17269. DOI:10.1021/acs.langmuir.4c01532
18. Mylkie K, Nowak P, Rybczynski P, Ziegler-Borowska M. Polymer-Coated Magnetite Nanoparticles for Protein Immobilization. *Materials* **2021**, *14*, 248. DOI:10.3390/ma14020248
19. Calsolaro F, Garello F, Cavallari E, Magnacca G, Trukhan MV, Valsania MC, et al. Amphoteric β-cyclodextrin coated iron oxide magnetic nanoparticles: New insights into synthesis and application in MRI. *Nanoscale Adv.* **2025**, *7*, 155–168. DOI:10.1039/d4na00692e
20. Alegbe EO, Uthman TO. A review of the history, properties, classification, applications and challenges of natural and synthetic dyes. *Heliyon* **2024**, *10*, e33646. DOI:10.1016/j.heliyon.2024.e33646
21. Benkhaya S, M'rabet S, El Harfi A. A review on classifications, recent synthesis and applications of textile dyes. *Inorg. Chem. Commun.* **2020**, *115*, 107891. DOI:10.1016/j.inoche.2020.107891
22. Niinimäki K, Peters G, Dahlbo H, Perry P, Rissanen T, Gwilt A. The environmental price of fast fashion. *Nat. Rev. Earth Environ.* **2020**, *1*, 189–200. DOI:10.1038/s43017-020-0039-9
23. Aponte NO, Gómez JH, Argüelles VT, Smith ED. Fast fashion consumption and its environmental impact: A literature review. *Sustain. Sci. Pract. Policy* **2024**, *20*, 2381871. DOI:10.1080/15487733.2024.2381871
24. Bazin I, Hassine AIH, Hamouda YH, Mnif W, Bartegi A, Lopez-Ferber M, et al. Estrogenic and anti-estrogenic activity of 23 commercial textile dyes. *Ecotoxicol. Environ. Saf.* **2012**, *85*, 131–136. DOI:10.1016/j.ecoenv.2012.08.003
25. Szejtli J. Introduction and General Overview of Cyclodextrin Chemistry. *Chem. Rev.* **1998**, *98*, 1743–1753. DOI:10.1021/cr970022c
26. Iacovino R, Caso JV, Di Donato C, Malgieri G, Palmieri M, Russo L, et al. Cyclodextrins as Complexing Agents: Preparation and Applications. *Curr. Org. Chem.* **2017**, *21*, 162–176. DOI:10.2174/1385272820666160909111842
27. Crini G. Review: A History of Cyclodextrins. *Chem. Rev.* **2014**, *114*, 10940–10975. DOI:10.1021/cr500081p
28. Morin-Crini N, Foumentin S, Fenyvesi E, Lichfouse E, Torri G, Foumentin M, et al. 130 years of cyclodextrin discovery for health, food, agriculture, and the industry: A review. *Environ. Chem.* **2021**, *19*, 2581–2617. DOI:10.1007/s10311-020-01156-w
29. Majd M, Yazdanpanah M, Beyatloo MR, Nojavan S. Recent advances and applications of cyclodextrins in magnetic solid phase extraction. *Talanta* **2021**, *219*, 122296. DOI:10.1016/j.talanta.2021.122296
30. Bezerra FM, Lis MJ, Firmino HB, Dias da Silva JG, Curto Valle RDCS, Borges Valle JA, et al. The Role of β-Cyclodextrin in the Textile Industry—Review. *Molecules* **2020**, *25*, 3624. DOI:10.3390/molecules25163624
31. Wagner BD. *Host-Guest Chemistry: Supramolecular Inclusion in Solution*; De Gruyer: Berlin, Germany, 2020.
32. He Y, Zhang L, Xiong HW, Kang X. Evolution of lattice defects in nickel ferrite spinel: Oxygen vacancy and cation substitution. *J. Alloys Compd*. **2022**, *917*, 165494. DOI:10.1016/j.jallcom.2022.165494
33. Rosencwaig A. Double Exchange and Electron Hopping in Magnetite. *Can. J. Phys.* **1969**, *47*, 2309–2317. DOI:10.1139/p69-281
34. Cuenca JA, Bugler K, Taylor S, Morgan D, Williams P, Bauer J, et al. Study of the magnetite to maghemite transition using microwave permittivity and permeability measurements. *J. Phys. Condens. Matter Phys.* **2016**, *28*, 106002. DOI:10.1088/0953-8984/28/10/106002
35. Niculescu AG, Chircov C, Grumezescu AM. Magnetite Nanoparticles: Synthesis Methods—A Comparative Review. *Methods* **2022**, *199*, 16–27. DOI:10.1016/j.ymeth.2021.04.018
36. Alonso J, Barandiarán JM, Fernández Barquín L, García-Arribas A. Magnetic Nanoparticles, Synthesis, Properties, and Applications. In *Magnetic Nanostructured Materials*; Elsevier: Amsterdam, The Netherlands, 2018; pp. 1–40. DOI:10.1016/B978-0-12-813904-2.00001-2
37. Gartmann N, Schütze C, Ritter H, Brühwiler D. The Effect of Water on the Functionalization of Mesoporous Silica with 3-Aminopropyltriethoxysilane. *J. Phys. Chem. Lett.* **2010**, *1*, 379–382. DOI:10.1021/jz9002795
38. Aberdeen S, Hur CA, Cal E, Vandeperre L, Ryan MP. Acid Resistant Functionalised Magnetic Nanoparticles for Radionuclide and Heavy Metal Adsorption. *J. Colloid Interface Sci.* **2022**, 608, 1728–1738. DOI:10.1016/j.jcis.2021.10.030
39. Chai W, Wang H, Zhang Y, Ding G. Preparation of Polydopamine-Coated Magnetic Nanoparticles for Dispersive Solid-Phase Extraction of Water-Soluble Synthetic Colorants in Beverage Samples with HPLC Analysis. *Talanta* **2016**, *149*, 13–20. DOI:10.1016/j.talanta.2015.11.026
40. Abdullah MMS, Faqihi NA, Al-Lohedan HA, Almarhoon ZM, Mohammad F. Fabrication of Magnetite Nanomaterials Employing Novel Ionic Liquids for Efficient Oil Spill Cleanup. *J. Environ. Manag.* **2022**, *316*, 115194–115205. DOI:10.1016/j.jenvman.2022.115194
41. Husain H, Hariyanto B, Sulthonul M, Klysubun W, Darminto D, Pratapa S. Structure and Magnetic Properties of Silica-

Coated Magnetite-Nanoparticle Composites. *Mater. Res. Express* **2019**, *6*, 086117. DOI:10.1088/2053-1591/ab29af
42. Yan H, Yu X, Dong G, Zhang Z, Ding K, Yang H, et al. Functionalized β-cyclodextrin with polyethyleneimine-coated Fe_3O_4 as a recyclable demulsifier for the efficient treatment of oily wastewater. *Colloids Surf. A Physicochem. Eng. Asp.* **2023**, *660*, 130877. DOI:10.1016/j.colsurfa.2022.130877
43. Li J, Wang Y, Dou X, Hao H, Dong S, Shao X, et al. Brilliant red X-3B uptake by a novel polycyclodextrin-modified magnetic cationic hydrogel: Performance, kinetics and mechanism. *J. Environ. Sci*. **2020**, *89*, 264–276. DOI:10.1016/j.jes.2019.09.008
44. Badruddoza AZM, Bhattarai B, Suri RPS. Environmentally Friendly β-Cyclodextrin−Ionic Liquid Polyurethane-Modified Magnetic Sorbent for the Removal of PFOA, PFOS, and Cr(VI) from Water. *ACS Sustain. Chem. Eng.* **2017**, *5*, 9223–9232. DOI:10.1021/acssuschemeng.7b02186
45. Cheng J, Chang PR, Zheng P, Ma X. Characterization of Magnetic Carbon Nanotube−Cyclodextrin Composite and Its Adsorption of Dye. *Ind. Eng. Chem. Res.* **2014**, *53*, 1415–1421. DOI:10.1021/ie402658x
46. Ouyang J, Gao J, Shen J, Wei Y, Wang C. Preparation of magnetic graphene/β-cyclodextrin polymer composites and their application for removal of organic pollutants from wastewater. *J. Environ. Chem. Eng.* **2023**, *11*, 110944. DOI:10.1016/j.jece.2023.110944
47. Salazar S, Yutronic N, Jara P. Magnetic β-Cyclodextrin Nanosponges for Potential Application in the Removal of the Neonicotinoid Dinotefuran from Wastewater. *Int. J. Mol. Sci.* **2020**, *21*, 4079. DOI:10.3390/ijms21114079
48. Hemmati M, Rajabi M, Asghari A. Magnetic nanoparticle based solid-phase extraction of heavy metal ions: A review on recent advances. *Microchim. Acta* **2018**, *185*, 160. DOI:10.1007/s00604-018-2670-4
49. Panda SK, Aggarwal I, Kumar H, Prasad L, Kumar A, Sharma A, et al. Magnetite nanoparticles as sorbents for dye removal: A review. *Environ. Chem. Lett.* **2021**, *19*, 2487–2525. DOI:10.1007/s10311-020-01173-9
50. Ghimire PP, Jaroniec M. Renaissance of Stöber method for synthesis of colloidal particles: New developments and opportunities. *J. Colloid Interface Sci.* **2021**, *584*, 838–865. DOI:10.1016/j.jcis.2020.10.014
51. Arslan M, Sayin S, Yilmaz M. Removal of Carcinogenic Azo Dyes from Water by New Cyclodextrin-Immobilized Iron Oxide Magnetic Nanoparticles. *Water Air Soil Pollut.* **2013**, *224*, 1527. DOI:10.1007/s11270-013-1527-z
52. Zhang Y, Wang W, Li Q, Yang Q, Li Y, Du J. Colorimetric magnetic microspheres as chemosensor for Cu^{2+} prepared from adamantane-modified rhodamine and β-cyclodextrin-modified Fe_3O_4@SiO_2 via host–guest interaction. *Talanta* **2015**, *141*, 33–40. DOI:10.1016/j.talanta.2015.03.015
53. Zhou Y, Sun L, Wang H, Liang W, Yang J, Wang L, et al. Investigation on the uptake and release ability of β-cyclodextrin functionalized Fe_3O_4 magnetic nanoparticles by methylene blue. *Mater. Chem. Phys.* **2016**, *170*, 83–89. DOI:10.1016/j.matchemphys.2015.12.022
54. Sedghi R, Yassari M, Heidari B. Thermo-responsive molecularly imprinted polymer containing magnetic nanoparticles: Synthesis, characterization and adsorption properties for curcumin. *Colloids Surf. B Biointerfaces* **2018**, *162*, 154–162. DOI:10.1016/j.colsurfb.2017.11.053
55. Shahrebabak SM, Saber-Tehrani M, Faraji M, Shabanian M, Aberoomand-Azar P. Magnetic solid phase extraction based on poly(β-cyclodextrin-ester) functionalized silica-coated magnetic nanoparticles (NPs) for simultaneous extraction of the malachite green and crystal violet from aqueous samples. *Environ. Monit. Assess.* **2020**, *192*, 262. DOI:10.1007/s10661-020-8185-6
56. Yadav M, Das M, Savani C, Thakore S, Jadeja R. Maleic Anhydride Cross-Linked β-Cyclodextrin-Conjugated Magnetic Nanoadsorbent: An Ecofriendly Approach for Simultaneous Adsorption of Hydrophilic and Hydrophobic Dyes. *ACS Omega* **2019**, *4*, 11993–112003. DOI:10.1021/acsomega.9b00881
57. Badruddoza AZM, Hazel GSS, Hidaget K, Uddin MS. Synthesis of carboxymethyl-β-cyclodextrin conjugated magnetic nano-absorbent for removal of methylene blue. *Colloids Surf. A Physicochem. Eng. Asp.* **2010**, *367*, 85–95. DOI:10.1016/j.colsurfa.2010.06.018
58. Li J, Chen C, Zhao Y, Hu J, Shao D, Wang X. Synthesis of water-dispersible Fe_3O_4@β-cyclodextrin by plasma-induced grafting technique for pollutant treatment. *Chem. Eng. J.* **2013**, *229*, 296–303. DOI:10.1016/j.cej.2013.06.016
59. Chen B, Chen S, Zhao H, Liu Y, Long F, Pan X. A versatile β-cyclodextrin and polyethyleneimine bi-functionalized magnetic nanoadsorbent for simultaneous capture of methyl orange and Pb(II) from complex wastewater. *Chemosphere* **2019**, *216*, 605–616. DOI:10.1016/j.chemosphere.2018.10.157
60. Liu D, Huang Z, Li M, Sun P, Yu T, Zhou L. Novel porous magnetic nanospheres functionalized by β-cyclodextrin polymer and its application in organic pollutants from aqueous solution. *Environ. Pollut.* **2019**, *250*, 639–649. DOI:10.1016/j.envpol.2019.04.079
61. Goshisht MK, Kaur R, Bakshi MS. Dye Extraction by Functionalized Magnetic Nanoparticles with Surfactants and Cyclodextrins through Specific and Host-Guest Interactions. *Lamgmuir* **2025**, *41*, 8214–8227.

DOI:10.1021/acs.langmuir.4c05340
62. Hu B, Hu Q, Hu J, Chen C. High-efficient capture of C.I. Basic Blue 3 by carboxymethyl-β-cyclodextrin conjugated magnetic composite. *Desalination Water Treat.* **2017**, *77*, 377–386. DOI:10.5004/dwt.2017.20836
63. Vahedi S, Tavakoli O, Khoobi M, Ansari A, Faramarzia MA. Application of novel magnetic β-cyclodextrin-anhydride polymer nano-adsorbent in cationic dye removal from aqueous solution. *J. Taiwan Inst. Chem. Eng.* **2017**, *807*, 452–463. DOI:10.1016/j.jtice.2017.07.039
64. Cai D, Zhang T, Zhang F, Luo X. Quaternary ammonium β-cyclodextrin-conjugated magnetic nanoparticles as nan-absorbents for the treatment of dyeing wastewater: Synthesis and adsorption studies. *J. Environ. Chem. Eng.* **2017**, *5*, 2869–2878. DOI:10.1016/j.jece.2017.06.001
65. Xie ZW, Lin JC, Xu MY, Wang HY, Wu YX, He F, et al. Novel Fe_3O_4 Nanoparticle/β-Cyclodextrin-Based Polymer Composites for the Removal of Methylene Blue from Water. *Ind. Eng. Chem. Res.* **2020**, *59*, 12270–12281. DOI:10.1021/acs.iecr.0c01115
66. Hu X, Hu Y, Xu G, Li M, Zhu Y, Jiang L, et al. Green synthesis of a magnetic β-cyclodextrin polymer for rapid removal of organic micro-pollutants and heavy metals from dyeing wastewater. *Environ. Res.* **2020**, *180*, 108796. DOI:10.1016/j.envres.2019.108796
67. Ning J, Chen D, Liu Y, Huang S, Wang F, Wei R, et al. Efficient adsorption removal and adsorption mechanism of basic fuchsin by recyclable Fe_3O_4@CD magnetic microspheres. *J. Cent. South Univ.* **2021**, *28*, 3666–3680. DOI:10.1007/s11771-021-4845-0
68. Lighvan ZM, Khonakdhar HA, Khodadadi B, Ramezanpour A, Rafie M, Heydari A, et al. Reduction of toxic organic dyes in aqueous media using *N*-heterocyclic copper(II) complex immobilized on the beta-cyclodextrin-modified Fe_3O_4 nanoparticles as a magnetically recyclable catalyst. *Res. Chem.* **2023**, *6*, 101021. DOI:10.1016/j.rechem.2023.101021
69. Liu B, Wang S, Wang H, Wang Y, Xiao Y, Cheng Y. Quaternary Ammonium Groups Modified Magnetic Cyclodextrin Polymers for Highly Efficient Dye Removal and Sterilization in Water Purification. *Molecules* **2023**, *28*, 167. DOI:10.3390/molecules28010167
70. Sabvezar AM, Ahmadpour A, Ghahramaninezhad M, Arami-Niya A. Tuning cross-linker type in the fabrication of beta-cyclodextrin/magnetic lignin adsorbents: Comparative study of cationic dye adsorption performance. *Environ. Technol. Innov.* **2025**, *40*, 104507. DOI:10.1016/j.eti.2025.104507
71. Sabvezar AM, Ahmadpour A, Ghahramaninezhad M. Preparation of beta-cyclodextrin decorated magnetic lignin by citric acid cross-linker for water treatment. *Carbohydr. Polym. Technol. Appl.* **2025**, *9*, 100654. DOI:10.1016/j.carpta.2024.100654
72. Al-Madhagi H, Yazbik V, Abdelwahed W, Alchab L. Magnetite Nanoparticle Co-precipitation Synthesis, Characterization, and Applications: Mini Review. *BioNanoScience* **2023**, *13*, 853–859. DOI:10.1007/s12668-023-01113-1
73. Fan L, Zhang Y, Luo C, Lu F, Qiu H, Sun M. Synthesis and characterization of magnetic β-cyclodextrin-chitosan nanoparticles as nano-adsorbents for removal of methyl blue. *Int. J. Biol. Macromol.* **2012**, *50*, 444–450. DOI:10.1016/j.ijbiomac.2011.12.016
74. Lv J, Zhai S, Fan Y, Lei Z, An Q. Preparation of β-CD and Fe_3O_4 integrated multifunctional bioadsorbent for highly efficient dye removal from water. *J. Taiwan Inst. Chem. Eng.* **2016**, *62*, 209–218. DOI:10.1016/j.jtice.2016.02.006
75. Ahmed Bakheet AA, Zhu X. Determination of Rhodamine B in Food Samples by Fe_3O_4@Ionic Liquids-β-Cyclodextrin Cross Linked Polymer Solid Phase Extraction Coupled with Fluorescence Spectrophotometry. *J. Fluoresc.* **2017**, *27*, 1087–1094. DOI:10.1007/s10895-017-2042-1
76. Kumari P, Parahara S, Parashara P. β-cyclodextrin modified magnetite nanoparticles for efficient removal of eosin and phloxine dyes from aqueous solution. *Mater. Today: Proc.* **2018**, *5*, 15473–15480. DOI:10.1016/j.matpr.2018.05.035
77. Nasiri S, Alizadeh N. Synthesis and adsorption behavior of hydroxypropyl-β-cyclodextrin–polyurethane magnetic nanoconjugates for crystal and methyl violet dyes removal from aqueous solutions. *RSC Adv.* **2019**, *9*, 24603–24616. DOI:10.1039/c9ra03335a
78. Yadav S, Asthana A, Chakraborty R, Jain B, Singh AK, Carabineiro SAC, et al. Cationic Dye Removal Using Novel Magnetic/Activated Charcoal/β-Cyclodextrin/Alginate Polymer Nanocomposite. *Nanomaterials* **2020**, *10*, 170. DOI:10.3390/nano10010170
79. Yadav S, Asthana A, Singh AK, Chakraborty R, Vidya SS, Susan MABH, et al. Adsorption of cationic dyes, drugs and metal from aqueous solutions using a polymer composite of magnetic/β-cyclodextrin/activated charcoal/Na alginate: Isotherm, kinetics and regeneration studies. *J. Hazard. Mater.* **2021**, *409*, 124840. DOI:10.1016/j.jhazmat.2020.124840
80. Rodriguez-López MI, Pellicer JA, Gómez-Morte T, Auñón D, Gómez-Lopez VM, Yánez-Gascön MJ, et al. Removal of an Azo Dye from Wastewater through the Use of Two Technologies: Magnetic Cyclodextrin Polymers and Pulsed Light. *Int. J. Mol. Sci.* **2022**, *23*, 8406. DOI:10.3390/ijms23158406

81. Chen T, Wen X, Li X, He J, Yan B, Fang Z, et al. Single/co-adsorption and mechanism of methylene blue and lead by β-cyclodextrin modified magnetic alginate/biochar. *Bioresour. Technol.* **2023**, *381*, 129130. DOI:10.1016/j.biortech.2023.129130
82. Fedorova O, Fedorov Y. Cyclodextrins as Supramolecular Hosts for Dye Molecules. In *Cyclodextrins—Core Concepts and New Frontiers*; IntechOpen: London, UK, 2023. DOI:10.5772/intechopen.107042
83. Moritz ED, Sahyun MRV. Spectroscopic studies of β-cyclodextrin-complexed cyanine dyes. *J. Photochem. Photobiol. A* **2005**, *169*, 211–220. DOI:10.1016/j.jphotochem.2004.06.020
84. Saifi A, Joseph JP, Singh AP, Pal A, Kumar K. Complexation of an Azo Dye by Cyclodextrins: A Potential Strategy for Water Purification. *ACS Omega* **2021**, *6*, 4776–4782. DOI:10.1021/acsomega.0c05684
85. Indirapriyadharshini VK, Karunanuthi P, Ramamurthy P. Inclusion of Resorcinal-Based Acridinedione Dyes in Cyclodextrins: Fluorescence Enhancement. *Lanmuir* **2001**, *17*, 4056–4060. DOI:10.1021/la0101200
86. Liu Y, Han BH, Chen YT. Molecular Recognition and Complexation Thermodynamics of Dye-Guest Molecules by Modified Cyclodextrins and Calixarenesulfonates. *J. Phys. Chem. B* **2002**, *106*, 46784687. DOI:10.1021/jp015603r
87. Barão CE, Pinheiro KH, Valarini O, Zanin GM, De Moraes FF. Determination of the Association Constant of Alpha and Beta Cyclodextrins using Methyl Orange. *Ind. Biotechnol.* **2016**, *12*, 317–322. DOI:10.1089/ind.2016.0009
88. Semerara P, Rizzi V, Fini P, Matero S, Cosma P, Franco E, et al. Interaction between industrial textile dyes and cyclodextrins. *Dyes Pigment.* **2015**, *119*, 84–94. DOI:10.1016/j.dyepig.2015.03.012
89. Scott J, Tidball A, Uitvlugt JM, Lucia M, Vander Griend DA, Louters LL. Methyl-β-cyclodextrin directly binds methylene blue and blocks both its cell staining and glucose uptake stimulatory effects. *Biochimie* **2009**, *91,* 271–276. DOI:10.1016/j.biochi.2008.10.003
90. Goyal N, Amar A, Gulati S, Varma RS. Cyclodextrin-Based Nanosponges as an Environmentally Sustainable Solution for Water Treatment: A Review. *ACS Appl. Nano Mater.* **2023**, *6*, 13766–13791. DOI:10.1021/acsanm.3c02026
91. Yadav R, Chundawat TS, Verma M, Vaya D. Utilizing Fe_2O_3-β-CD magnetic nanocomposite for efficient removal of MG dye and Gunner 500 pesticide from wastewater. *Inorg. Chem. Commun.* **2024**, *170*, 113416. DOI:10.1016/j.inoche.2024.113416
92. Kaur N, Junega B, Ballal S, Prasad GVS, Nanda A, Kaur M, et al. Greener and efficient magnetic CS-Fe_2O_3 nanocomposite fabricated with β-Cyclodextrin for wastewater treatment: Heavy metal adsorption and photocatalytic degradation of industrial dyes. *J. Mol. Struct.* **2025**, *1328*, 141310. DOI:10.1016/j.molstruc.2024.141310
93. Ahmed A, Usman M, Yu B, Gao F, Shen Y, Cong H. Heterogeneous activation of peroxymonosulfate using superparamagnetic β-CD-$CoFe_2O_4$ catalyst for the removal of endocrine-disrupting bisphenol A: Performance and degradation mechanism. *Sep. Purif. Technol.* **2021**, *279*, 119752. DOI:10.1016/j.seppur.2021.119752
94. Qin D, Hu W, Zhang L. Green synthesis of β-cyclodextrin conjugated Fe_3O_4/NiO nanocomposites and its synergistic effect of adsorption and photocatalytic degradation for Congo red removal. *Desalination Water Treat.* **2024**, *317*, 100136. DOI:10.1016/j.dwt.2024.100136
95. Singh BK, Pande PP, Chaurasiya A, Dey KK, Kushwaha N. Synthesis and characterisation of novel β-cyclodextrin based Fe_3O_4 nanocomposite; adsorption behaviour and photocatalytic dye degradation studies. *Int. J. Environ. Anal. Chem.* **2025**, *105*, 4587–4612. DOI:10.1080/03067319.2024.2373358